https://doi.org/10.5194/hess-2020-87
Preprint. Discussion started: 10 March 2020

Hydrology and Earth System Sciences
Discussions

Hierarchical Sensitivity Analysis for Large-scale Process-based Hydrological Modeling with Application in an Amazonian Watershed

Haifan Liu[1], Heng Dai[2*], Jie Niu[2*], Bill X. Hu[2], Han Qiu[3], Dongwei Gui[4], Ming Ye[5], Xingyuan Chen[6], Chuanhao Wu[2], Jin Zhang[2], and William Riley[7]

[1]School of Water Resources and Environment, China University of Geosciences, Beijing, 100083, China.
[2]Institute of Groundwater and Earth Sciences, Jinan University, Guangzhou 510632, China.
[3]State Key Laboratory of Desert and Oasis Ecology, Xinjiang Institute of Ecology and Geography, Chinese Academy of Sciences, Urumqi 830011, China
[4]Department of Civil and Environmental Engineering, Michigan State University, East Lansing, MI. USA.
[5]Department of Earth, Ocean, and Atmospheric Science, Florida State University, Tallahassee, FL 32306, USA.
[6]Pacific Northwest National Laboratory, Richland, WA 99352, USA.
[7]Earth Sciences Division, Lawrence Berkeley National Laboratory, Berkeley, California, USA.

Correspondence to: Heng Dai (heng.dai@jnu.edu.cn) and Jie Niu (jniu@jnu.edu.cn)

Abstract. Sensitivity analysis is an effective tool for identifying important uncertainty sources and improving model calibration and predictions, especially for integrated systems with heterogeneous parameter inputs and complex process coevolution. In this work, an advanced hierarchical global sensitivity analysis framework, which integrates the concept of variance-based global sensitivity analysis with a hierarchical uncertainty framework, was implemented to quantitatively analyse several uncertainties associated with a three-dimensional, process-based hydrologic model (PAWS). The uncertainty sources considered include model parameters (three vadose zone parameters, two groundwater parameters, and one overland flow parameter), model structure (different thicknesses to represent unconfined and confined aquifer layers) and climate scenarios. We apply the approach to an ~9,000 km^2 Amazon catchment modeled at 1 km resolution to provide a demonstration of multiple uncertainty source quantification using a large-scale process-based hydrologic model. The sensitivity indices are assessed based on two important hydrologic outputs: evapotranspiration (*ET*) and groundwater contribution to streamflow (Q_G). It was found that, in general, parameters, especially the vadose zone parameters, are the most important uncertainty contributors for all sensitivity indices. In addition, the influence of climate scenarios on *ET* predictions is also nonignorable. Furthermore, the thickness of the aquifers along the river grid cells is important for both *ET* and Q_G. These results can assist in model calibration and provide modelers with a better understanding of the general sources of uncertainty in predictions associated with complex hydrological systems in Amazonia. We demonstrated a pilot example of comprehensive global sensitivity analysis of large-scale, complex hydrological and environmental models in this study. The hierarchical sensitivity analysis methodology used is mathematically rigorous and capable of being implemented in a variety of large-scale hydrological models with various sources of uncertainty.

https://doi.org/10.5194/hess-2020-87
Preprint. Discussion started: 10 March 2020


Hydrology and Earth System Sciences
Discussions

1 Introduction

Large-scale three-dimensional process-based hydrological models (PBHMs) are being increasingly applied not only to evaluate watershed hydrologic responses to climate forcing but also to understand ecosystem energy balance, biogeochemistry, and ecological functioning from basin to continental scales (Shen et al., 2013; Maxwell et al., 2014; Riley and Shen 2014). PBHMs can simulate the interacting states and fluxes of integrated surface and subsurface hydrological processes and accurately predict large-scale complex hydrologic system behaviours (Niu et al., 2014; Shen et al., 2014; Niu and Phanikumar, 2015; Niu et al., 2017). Distributed flow pathways, e.g., evapotranspiration (*ET*), overland flow, channel runoff, etc., can be distinguished by PBHM simulations (Beven, 2002). In addition, the governing equations for subsurface flow are explicitly solved in PBHMs; thus, they can simulate detailed hydrological processes, including root extraction, infiltration, soil evaporation, and groundwater discharge and recharge in the vadose zone (Maxwell et al., 2014). However, the complexities and uncertainties inherent in PBHM structures, heterogeneous model parameters, heterogeneous data sources (e.g., elevation, soil properties, groundwater conductivities), and climate forcing may produce high uncertainties in the modeling outputs (Shen et al., 2014; Qiu et al., 2019). Uncertainty in numerical modeling is inevitable and important (Neuman, 2003; Rojas et al., 2010), especially for PBHMs that represent a high level of physical process complexity. Sensitivity analysis becomes important to identify the most influential sources of uncertainty so that limited resources can be used to maximally reduce model predictive uncertainty (Neuman, 2003; Saltelli et al., 2010; Lu et al., 2012; Song et al., 2015).

In general, sensitivity analysis can be separated into local and global methods. The main limitation of local sensitivity analysis is that its results are only valid for a small range of parameter values (Gedeon et al., 2012; King and Perera, 2013; Wainwright et al., 2014; Dai and Ye, 2015). Compared to the local method, global sensitivity analysis can provide sensitivity estimates for the entire range of uncertain parameter values (Saltelli et al., 2000, 2010; Razavi and Gupta 2015, 2016). Because of this advantage, global sensitivity analysis has gained popularity in recent modeling analyses despite its high computational cost (Hamby, 1994; van Griensven et al., 2006; Sulis et al., 2011; Baroni et al., 2014). Among different global sensitivity analysis methods, the variance-based method has been widely used because of its ability to accurately quantify the importance of uncertain parameters while considering their interactions (Saltelli and Sobol, 1995; Zhang et al., 2013; Dai and Ye, 2015).

There is still a lack of research utilizing quantitative and representative global sensitivity analysis using large-scale PBHMs due to the high computational cost (Emery et al., 2016). Most sensitivity analysis research pertaining to hydrological models has used local sensitivity analysis methods (Chavarri et al., 2013; de Paiva et al., 2013; Nijssen et al., 2001). Moreover, conventional global sensitivity analysis includes only the uncertainty from model parameters and ignores other important sources of hydrological model uncertainty, including scenario uncertainty caused by alternative unpredictable future climate conditions (e.g., precipitation, radiation intensity, temperature, humidity, and wind speed) and structural uncertainty caused

https://doi.org/10.5194/hess-2020-87
Preprint. Discussion started: 10 March 2020


Hydrology and Earth System Sciences
Discussions

by different interpretations of the real situation and reflecting on the plausible models (Ye et al., 2005; Makler-Pick et al., 2011; Neumann, 2012; Dai and Ye, 2015; Song et al., 2015; Dai et al., 2017a,b).

In this study, we applied an advanced hierarchical global sensitivity analysis approach to a PBHM (the process-based adaptive watershed simulator; PAWS) for a watershed in the Amazon considering multiple uncertainty sources. Hierarchical sensitivity analysis was first proposed by Dai and Ye (2015) and then applied to a groundwater modeling analysis for the Hanford 300 Area in Washington, U.S. (Dai et al., 2017a). The hierarchical sensitivity analysis method integrates the concept of variance-based global sensitivity analysis with the hierarchical uncertainty quantification framework (Draper et al., 1999; Dai and Ye, 2015) to quantify the sensitivity of important processes to model parametric and structural uncertainty. This advanced sensitivity analysis method considers three important sources of uncertainty (i.e., scenario, structural, and parametric) involved in hydrological models and dramatically decreases computational costs by combining uncertain inputs based on their characteristics and interdependencies. We also improved the hierarchical sensitivity analysis methodology by introducing new parameter groups into the uncertainty framework and implementing new algorithms to make the assessment of global sensitivity analysis for large-scale PBHMs computationally affordable. This study is the first to implement a comprehensive hierarchical sensitivity analysis method in relation to a complex and large-scale PBHM. In this study, we revised the hierarchical sensitivity analysis method and defined a set of sensitivity indices to group and accurately quantify the importance of different uncertainty sources in PAWS when simulating hydrological processes in an Amazonian watershed.

PAWS has been applied extensively in many watersheds, e.g., the large watersheds in Michigan state, U.S. (Niu et al., 2014, 2017; Ji et al., 2015; Shen et al., 2013, 2014, 2016; Qiu et al., 2019), and the watershed in the Amazon basin (Niu et al., 2017), and demonstrates high efficiency and good performance. Here, we applied PAWS to the Amazon because this region includes more than half of the tropical rainforests globally (Morley, 2000) and plays an essential role in the world carbon (Richey et al., 2002; Phillips et al., 2009; Lintner et al., 2017) and water (Fearnside, 2005; Phillips et al., 2009) cycles. Amazonian forest hydrology can affect many processes, including nutrient budgets (Lesack and Melack 1996), the production and consumption of carbohydrates (Pegoraro et al., 2006), and root-zone moisture availability for plants (Oliveira et al., 2005; Tang et al., 2015). A large number of field (Lesack 1993; Leopoldo et al., 1995; Tomasella et al., 2008) and numerical modeling (Coe et al., 2008; Sorribas et al., 2016; Yamazaki et al., 2012) studies have been performed to improve our understanding of hydrologic processes in the Amazon. As some studies have indicated that groundwater is the key controller of Amazon hydrology (Leopoldo et al., 1995; Hodnett et al., 1997a,b; Beighley et al., 2009; Pokhrel et al., 2014; Niu et al., 2017), some researchers have already implemented simulations involving subsurface water in the Amazon (Miguez-Macho and Fan, 2012a,b). The severe hydrological hazards that frequently occurred in the Amazon in the past, such as the droughts in 2005 and 2010 and the floods of 2009 (Tomasella et al., 2008; Marengo et al., 2010; Espinoza et al., 2011), also increase the requirement of including climate scenario uncertainty and related model uncertainty in sensitivity analyses for the Amazon region.

https://doi.org/10.5194/hess-2020-87
Preprint. Discussion started: 10 March 2020


Hydrology and Earth System Sciences
Discussions

The PAWS model applied in this work was originally used in Niu et al. (2017) to simulate the hydrologic cycle in an Amazonian watershed. Here, we build on that work by classifying model system uncertainty sources into three groups: uncertainty related to climate scenarios (six climate scenarios that differ in terms of radiation, precipitation, temperature, humidity, and wind speed), model structure (different thicknesses to represent aquifers), and parameters, including soil saturated hydraulic conductivity, K_s (m day^{-1}), the Van Genuchten equation parameters α (m^{-1}) and N (unitless) (van Genuchten, 1980), unconfined aquifer hydraulic conductivity, K_1 (m day^{-1}), confined aquifer hydraulic conductivity, K_2 (m day^{-1}), and length of flow path for runoff contribution to overland flow domain, L (m). We consider the Van Genuchten parameters α and N here because the correlation between α and N can largely affect the soil water release and infiltration processes in the vadose zone (Pan et al., 2011). A new set of subdivided parametric sensitivity indices was first defined to provide more detailed information for parametric sensitivities. Because of the high complexity and dimensionality of this model, the highly efficient parameter sampling method of Latin hypercube sampling (LHS) and a binning method were applied to estimate the sensitivity indices. We also investigated the effects of prior weights on the climate scenarios and numerical models. By implementing the hierarchical sensitivity analysis method, we aim to provide a pilot example of comprehensive global sensitivity analysis for large-scale PBHMs considering all uncertainty sources instead of only parameters and investigate the most important source of uncertainty for modeling hydrological processes in the Amazon.

We introduce the study area and the numerical model in Section 2.1. Sections 2.2 and 2.3 present the hierarchical sensitivity analysis method and its algorithms in detail. Then, we describe the definition and generation of uncertainty sources based on the study site information in Section 2.4. We present and discuss the results in Section 3. Section 4 summarizes the key findings of this research.

2 Materials and methods

2.1 Study site and numerical model

The study site is located in northern Manaus, Brazil (Fig. 1), with a drainage area of ~9,000 km^2. Within the central Amazon, the watershed is mostly covered by tropical forest, with ~12% cropland and ~5% wetland (based on Community Land Model (CLM) land surface data; Niu et al., 2017). With the relatively high elevation (90 – 210 m) of the upper landscape and the relatively low elevation (45 – 55 m) of the swampy valleys, a dense drainage network was formed in the region. The watershed has 4 rivers: the Urubu, Preto da Eva, Tarumã-açu, and Tarumã-mirim rivers. The average precipitation in this region has large seasonal variability. From December to May is the wet season, while from June to November is the dry season.

The model tool used in this study is the PAWS model (Niu et al., 2017), which implements an effective non-iterative scheme to couple hydrologic processes including both land surface and subsurface water. The details of the numerical implementation and the governing equations of PAWS can be found in Appendix A. Briefly, four flow domains are

https://doi.org/10.5194/hess-2020-87
Preprint. Discussion started: 10 March 2020


Hydrology and Earth System Sciences
Discussions

simulated in PAWS, including the stream channel, overland flow, the vadose zone, and saturated groundwater. The structured grid-based finite-volume method is the main numerical scheme applied to discretize the governing equations of the various hydrologic components. PAWS also simulates two land surface subdomains, i.e., infiltration and evaporation, which are depicted in the ponding subdomain, while overland flow occurs in the surface flow subdomain. PAWS considers the horizontal interaction of both surface runoff and groundwater flow between the model grids, which represents the actual hydrological processes and is often ignored by other regional and global hydrologic models. The 1-D diffusive wave equation is solved to simulate channel flow, and the 2-D version is used for overland flow. The leakance concept is the basis applied to explicitly simulate the exchange between the channel and groundwater. PAWS has been coupled with the CLM (Shen et al., 2013), which calculates the surface energy balance and soil and plant carbon and nitrogen cycles. Canopy interception and *ET* demand (both transpiration and soil evaporation) are also computed in the CLM at each time step.

For the numerical model case in this study, a 1 km × 1 km grid is used for horizontal discretization, resulting in 118 × 122 grid cells for the study site. In this model, 20 vertical layers were defined to discretize the vadose zone, and for the fully saturated groundwater, there are two layers: the unconfined aquifer on the top and the confined aquifer at the bottom.

In this study, 90 m resolution NASA Shuttle Radar Topography Mission (SRTM) (U.S. Geological Survey; http://eros.usgs.gov) data are applied as DEM input, but for the channel network and watershed boundary delineation, the Advanced Spaceborne Thermal Emission and Reflection Radiometer (ASTER) provides the 30 m resolution Global Digital Elevation Model Version 2 (GDEM V2) instead. CLM land surface data are applied as land use and land cover (LULC) inputs. Details regarding these data can be found in Niu et al. (2017). More information on the governing equations of PAWS can be found in Shen and Phanikumar (2010) and Niu et al. (2014).

2.2 Hierarchical sensitivity analysis method

The essential concept of the hierarchical sensitivity analysis method involves categorizing and quantifying different complex uncertainties of certain model systems while considering their dependence relationships. Different uncertainty sources (or uncertain inputs) are placed at different layers of a hierarchical uncertainty framework, which is then integrated with the variance-based global sensitivity analysis method to form a new set of sensitivity indices to accurately quantify the importance of different uncertainty sources.

In this study, we implemented the hierarchical sensitivity analysis method to assess the sensitivity of a large-scale process-based hydrological model, PAWS, with uncertainty from climate scenarios, numerical models and parameters. Similar to the work of Dai et al. (2017a), there are also three layers of uncertainties in the hierarchical uncertainty framework constructed for this research, including the upper layer of scenario uncertainty, the middle layer of model uncertainty, and the bottom layer of parameter uncertainty (Fig. 2). However, unlike the previous work, we further decomposed the layer of parametric uncertainty into three groups of uncertainties to investigate the importance of different uncertain parameters (Fig. 2). All of

https://doi.org/10.5194/hess-2020-87
Preprint. Discussion started: 10 March 2020


Hydrology and Earth System Sciences
Discussions

these uncertainties were placed into the proper levels based on their dependence relationships. Climate scenario uncertainties were placed on the first layer because the climate scenarios (differing in precipitation, radiation, temperature, humidity, and wind speed) are the driving forces of the model system, multiple models can be built under a single scenario, and the choice of models depends on the characteristics of the scenarios. The second layer includes the numerical model uncertainties, which represent different plausible mathematical conceptualizations describing the study site. In this study, they represent three models with different aquifer thicknesses. Under each climate scenario, these three models are likely to coexist. Parametric uncertainty is included in the bottom layer because each model can contain a different set of parameters (Meyer et al., 2007). Note that in Fig. 2, the term **PR** represents the multiple parameter sets under a certain numerical model. In the following content, we will introduce the revised mathematical formulas involved in the hierarchical sensitivity analysis method used in this study.

For the model: $\boldsymbol{\Delta} = f(X) = f(X_1,...,X_m)$, where $\boldsymbol{\Delta}$ is the model output and $X = \{X_1,...,X_m\}$ is a group of uncertainty inputs, using the law of total variance, the total variance of $\boldsymbol{\Delta}$ can be decomposed as (Dai and Ye, 2015):

$$V(\boldsymbol{\Delta}) = V_{X_i}\left(E_{\mathbf{X}_{\sim i}}\left(\boldsymbol{\Delta}|X_i\right)\right) + E_{X_i}\left(V_{\mathbf{X}_{\sim i}}\left(\boldsymbol{\Delta}|X_i\right)\right), \quad (1)$$

where the first term of partial variance on the right-hand side is the within-X_i partial variance and represents the variance contribution by X_i and $\mathbf{X}_{\sim i}$ represents all the inputs except X_i. The second term on the right-hand side represents the variance contributed by the model inputs excluding X_i as well as the interactions of all the inputs. Based on the definition of the first-order sensitivity index $S_i = \frac{V_{X_i}(E_{\mathbf{X}_{\sim i}}(\Delta \mid X_i))}{V(\Delta)}$ (Saltelli et al., 1995), the percentage of uncertainty contributed by input X_i can be accurately quantified.

Using the hierarchical framework in Fig. 2, the variance-based sensitivity analysis method enables the decomposition of the total variance into individual contributors as follows:

$$\begin{aligned} V(\boldsymbol{\Delta}) &= V_{\mathbf{CS}}\left(E_{\sim \mathbf{CS}|\mathbf{CS}}\left(\boldsymbol{\Delta}|\mathbf{CS}\right)\right) + E_{\mathbf{CS}}\left(V_{\sim \mathbf{CS}|\mathbf{CS}}\left(\boldsymbol{\Delta}|\mathbf{CS}\right)\right) \\ &= V_{\mathbf{CS}}\left(E_{\mathbf{NM,\,PR}|\mathbf{CS}}\left(\boldsymbol{\Delta}|\mathbf{CS}\right)\right) + E_{\mathbf{CS}}\left(V_{\mathbf{NM,\,PR}|\mathbf{CS}}\left(\boldsymbol{\Delta}|\mathbf{CS}\right)\right), \end{aligned} \quad (2)$$

where **CS** represents the set of alternative climate scenarios and **NM** represents the multiple plausible numerical models, **PR**, is the uncertain parameter. The term ~**CS** represents the uncertain inputs excluding climate scenarios, which are **NM** and **PR** in this study. The term **NM, PR**|**CS** represents the change in the combination of the model and parameters under one fixed climate scenario. The first term of partial variance on the right-hand side of this equation represents the variance caused by multiple climate scenarios. The second term on the right-hand side is the partial variance caused by other uncertain inputs and can be further decomposed as:

https://doi.org/10.5194/hess-2020-87
Preprint. Discussion started: 10 March 2020


Hydrology and Earth System Sciences
Discussions

$$V_{\mathbf{NM,\,PR|CS}}\left(\mathbf{\Delta|CS}\right)=V_{\mathbf{NM|CS}}\left(E_{\mathbf{PR|NM,\,CS}}\left(\mathbf{\Delta|NM,\,CS}\right)\right)+E_{\mathbf{NM|CS}}\left(V_{\mathbf{PR|NM,\,CS}}\left(\mathbf{\Delta|NM,\,CS}\right)\right), \tag{3}$$

where the first partial variance term on the right-hand side of this equation represents the uncertainty contributed by multiple plausible models. The subscripts **NM|CS** and **PR|NM, CS** refer to the change in the models under one climate scenario and the change in the parameters under one model and climate scenario, respectively. The second term represents the within-model partial variance caused by the uncertain parameters. By substituting Eq. (3) back into Eq. (2), we can obtain:

$$\begin{aligned} V\left(\mathbf{\Delta}\right) &= E_{\mathbf{CS}}\left(E_{\mathbf{NM|CS}}V_{\mathbf{PR|NM,\,CS}}\left(\mathbf{\Delta\,|\,NM,\,CS}\right)+V_{\mathbf{NM|CS}}E_{\mathbf{PR|NM,\,CS}}\left(\mathbf{\Delta\,|\,NM,\,CS}\right)\right) \\ &\quad +V_{\mathbf{CS}}E_{\mathbf{NM|CS}}E_{\mathbf{PR|NM,\,CS}}\left(\mathbf{\Delta\,|\,NM,\,CS}\right) \\ &= E_{\mathbf{CS}}E_{\mathbf{NM|CS}}V_{\mathbf{PR|NM,\,CS}}\left(\mathbf{\Delta\,|\,NM,\,CS}\right)+E_{\mathbf{CS}}V_{\mathbf{NM|CS}}E_{\mathbf{PR|NM,\,CS}}\left(\mathbf{\Delta\,|\,NM,\,CS}\right) \\ &\quad +V_{\mathbf{CS}}E_{\mathbf{NM|CS}}E_{\mathbf{PR|NM,\,CS}}\left(\mathbf{\Delta\,|\,NM,\,CS}\right) \\ &= V\left(\mathbf{PR}\right)+V\left(\mathbf{NM}\right)+V\left(\mathbf{CS}\right) \end{aligned}. \tag{4}$$

The three terms on the right-hand side of Eq. (4) represent the partial variances contributed by the parameters, models and climate scenarios, respectively. The equation indicates that the total variance can be decomposed into the variances contributed by the alternative climate scenarios, **CS**, plausible numerical models, **NM**, and uncertain parameters, **PR**. Then, we can define the new sensitivity indices for **PR**, **NM** and **CS** following the first-order sensitivity index definition (Dai et al., 2017a):

$$S_{\mathbf{PR}}=\frac{E_{\mathbf{CS}}E_{\mathbf{NM|CS}}V_{\mathbf{PR|NM,\,CS}}\left(\mathbf{\Delta\,|\,NM,\,CS}\right)}{V\left(\mathbf{\Delta}\right)}=\frac{V\left(\mathbf{PR}\right)}{V\left(\mathbf{\Delta}\right)}, \tag{5}$$

$$S_{\mathbf{NM}}=\frac{E_{\mathbf{CS}}V_{\mathbf{NM|CS}}E_{\mathbf{PR|NM,\,CS}}\left(\mathbf{\Delta\,|\,NM,\,CS}\right)}{V\left(\mathbf{\Delta}\right)}=\frac{V\left(\mathbf{NM}\right)}{V\left(\mathbf{\Delta}\right)}, \tag{6}$$

$$S_{\mathbf{CS}}=\frac{V_{\mathbf{CS}}E_{\mathbf{NM,\,CS}}E_{\mathbf{PR|NM,\,CS}}\left(\mathbf{\Delta\,|\,NM,\,CS}\right)}{V\left(\mathbf{\Delta}\right)}=\frac{V\left(\mathbf{CS}\right)}{V\left(\mathbf{\Delta}\right)}. \tag{7}$$

In this study, the partial variance of the parameters was further decomposed to assess the subdivided parametric sensitivities contributed by the vadose zone parameters ($\mathbf{PR}_{\mathrm{VDZ}}$), groundwater parameters ($\mathbf{PR}_{\mathrm{GW}}$) and overland flow parameter ($\mathbf{PR}_{\mathrm{OVN}}$). Using the total variance decomposition method, the partial variance of the parameters can be further decomposed as:

https://doi.org/10.5194/hess-2020-87
Preprint. Discussion started: 10 March 2020

Hydrology and Earth System Sciences
Discussions

$$
\begin{aligned}
V(\mathbf{PR}) &= E_{\mathbf{CS}} E_{\mathbf{NM|CS}} V_{\mathbf{PR|NM,CS}} \left(\mathbf{\Delta} \mid \mathbf{NM, CS}\right) \\
&= E_{\mathbf{CS}} E_{\mathbf{NM|CS}} \begin{pmatrix} V_{\mathbf{PR}_{\mathrm{VDZ}}\mid \mathbf{NM,CS}} \left(E_{\mathbf{PR}_{\sim \mathrm{VDZ}}\mid \mathbf{PR}_{\mathrm{VDZ}}, \mathbf{NM,CS}} \left(\mathbf{\Delta} \mid \mathbf{PR}_{\mathrm{VDZ}}, \mathbf{NM, CS}\right)\right) + \\ E_{\mathbf{PR}_{\mathrm{VDZ}}\mid \mathbf{NM,CS}} \left(V_{\mathbf{PR}_{\sim \mathrm{VDZ}}\mid \mathbf{PR}_{\mathrm{VDZ}}, \mathbf{NM,CS}} \left(\mathbf{\Delta} \mid \mathbf{PR}_{\mathrm{VDZ}}, \mathbf{NM, CS}\right)\right) \end{pmatrix}. \\
&= E_{\mathbf{CS}} E_{\mathbf{NM|CS}} V_{\mathbf{PR}_{\mathrm{VDZ}}\mid \mathbf{NM,CS}} E_{\mathbf{PR}_{\mathrm{GW}}, \mathbf{PR}_{\mathrm{OVN}}\mid \mathbf{PR}_{\mathrm{VDZ}}, \mathbf{NM,CS}} \left(\mathbf{\Delta} \mid \mathbf{PR}_{\mathrm{VDZ}}, \mathbf{NM, CS}\right) \\
&+ E_{\mathbf{CS}} E_{\mathbf{NM|CS}} E_{\mathbf{PR}_{\mathrm{VDZ}}\mid \mathbf{NM,CS}} V_{\mathbf{PR}_{\mathrm{GW}}, \mathbf{PR}_{\mathrm{OVN}}\mid \mathbf{PR}_{\mathrm{VDZ}}, \mathbf{NM,CS}} \left(\mathbf{\Delta} \mid \mathbf{PR}_{\mathrm{VDZ}}, \mathbf{NM, CS}\right)
\end{aligned} \tag{8}
$$

The subscript $\mathbf{PR}_{\mathrm{VDZ}}\mathbf{|NM, CS}$ represents the change in vadose zone parameters under a fixed model and climate scenarios. The subscript $\mathbf{PR}_{\sim \mathrm{VDZ}}\mathbf{|PR}_{\mathrm{VDZ}}\mathbf{, NM, CS}$ refers to other uncertain parameter inputs excluding vadose zone parameters, which are groundwater parameters and the overland flow parameter. The first term of Eq. (8) on the right-hand side is the partial variance of $\mathbf{PR}_{\mathrm{VDZ}}$, and the second term represents the partial variance of the other parameters, which are groundwater parameters and the overland flow parameter. Note that Eq. (8) is decomposed at the level of vadose zone parameters; when we decompose the partial variance of parameters at the level of groundwater parameters or the overland flow parameter, the partial variance of the parameters can be expressed as Eq. (9) and Eq. (10):

$$
\begin{aligned}
V(\mathbf{PR}) &= E_{\mathbf{CS}} E_{\mathbf{NM|CS}} V_{\mathbf{PR|NM,CS}} \left(\mathbf{\Delta} \mid \mathbf{NM, CS}\right) \\
&= E_{\mathbf{CS}} E_{\mathbf{NM|CS}} \begin{pmatrix} V_{\mathbf{PR}_{\mathrm{GW}}\mid \mathbf{NM,CS}} \left(E_{\mathbf{PR}_{\sim \mathrm{GW}}\mid \mathbf{PR}_{\mathrm{GW}}, \mathbf{NM,CS}} \left(\mathbf{\Delta} \mid \mathbf{PR}_{\mathrm{GW}}, \mathbf{NM, CS}\right)\right) + \\ E_{\mathbf{PR}_{\mathrm{GW}}\mid \mathbf{NM,CS}} \left(V_{\mathbf{PR}_{\sim \mathrm{GW}}\mid \mathbf{PR}_{\mathrm{GW}}, \mathbf{NM,CS}} \left(\mathbf{\Delta} \mid \mathbf{PR}_{\mathrm{GW}}, \mathbf{NM, CS}\right)\right) \end{pmatrix}, \\
&= E_{\mathbf{CS}} E_{\mathbf{NM|CS}} V_{\mathbf{PR}_{\mathrm{GW}}\mid \mathbf{NM,CS}} E_{\mathbf{PR}_{\mathrm{VDZ}}, \mathbf{PR}_{\mathrm{OVN}}\mid \mathbf{PR}_{\mathrm{GW}}, \mathbf{NM,CS}} \left(\mathbf{\Delta} \mid \mathbf{PR}_{\mathrm{GW}}, \mathbf{NM, CS}\right) \\
&+ E_{\mathbf{CS}} E_{\mathbf{NM|CS}} E_{\mathbf{PR}_{\mathrm{GW}}\mid \mathbf{NM,CS}} V_{\mathbf{PR}_{\mathrm{VDZ}}, \mathbf{PR}_{\mathrm{OVN}}\mid \mathbf{PR}_{\mathrm{GW}}, \mathbf{NM,CS}} \left(\mathbf{\Delta} \mid \mathbf{PR}_{\mathrm{GW}}, \mathbf{NM, CS}\right)
\end{aligned} \tag{9}
$$

$$
\begin{aligned}
V(\mathbf{PR}) &= E_{\mathbf{CS}} E_{\mathbf{NM|CS}} V_{\mathbf{PR|NM,CS}} \left(\mathbf{\Delta} \mid \mathbf{NM, CS}\right) \\
&= E_{\mathbf{CS}} E_{\mathbf{NM|CS}} \begin{pmatrix} V_{\mathbf{PR}_{\mathrm{OVN}}\mid \mathbf{NM,CS}} \left(E_{\mathbf{PR}_{\sim \mathrm{OVN}}\mid \mathbf{PR}_{\mathrm{OVN}}, \mathbf{NM,CS}} \left(\mathbf{\Delta} \mid \mathbf{PR}_{\mathrm{OVN}}, \mathbf{NM, CS}\right)\right) + \\ E_{\mathbf{PR}_{\mathrm{OVN}}\mid \mathbf{NM,CS}} \left(V_{\mathbf{PR}_{\sim \mathrm{OVN}}\mid \mathbf{PR}_{\mathrm{OVN}}, \mathbf{NM,CS}} \left(\mathbf{\Delta} \mid \mathbf{PR}_{\mathrm{OVN}}, \mathbf{NM, CS}\right)\right) \end{pmatrix}. \\
&= E_{\mathbf{CS}} E_{\mathbf{NM|CS}} V_{\mathbf{PR}_{\mathrm{OVN}}\mid \mathbf{NM,CS}} E_{\mathbf{PR}_{\mathrm{VDZ}}, \mathbf{PR}_{\mathrm{GW}}\mid \mathbf{PR}_{\mathrm{OVN}}, \mathbf{NM,CS}} \left(\mathbf{\Delta} \mid \mathbf{PR}_{\mathrm{OVN}}, \mathbf{NM, CS}\right) \\
&+ E_{\mathbf{CS}} E_{\mathbf{NM|CS}} E_{\mathbf{PR}_{\mathrm{OVN}}\mid \mathbf{NM,CS}} V_{\mathbf{PR}_{\mathrm{VDZ}}, \mathbf{PR}_{\mathrm{GW}}\mid \mathbf{PR}_{\mathrm{OVN}}, \mathbf{NM,CS}} \left(\mathbf{\Delta} \mid \mathbf{PR}_{\mathrm{OVN}}, \mathbf{NM, CS}\right)
\end{aligned} \tag{10}
$$

The first term of Eq. (9) and (10) represents the partial variance contributed by the groundwater and overland flow parameters, respectively. Then, we can define the sensitivity indices for $\mathbf{PR}_{\mathrm{VDZ}}$, $\mathbf{PR}_{\mathrm{GW}}$ and $\mathbf{PR}_{\mathrm{OVN}}$ following the first-order sensitivity index definition:

$$
S_{\mathbf{PR}_{\mathrm{VDZ}}} = \frac{E_{\mathbf{CS}} E_{\mathbf{NM|CS}} V_{\mathbf{PR}_{\mathrm{VDZ}}\mid \mathbf{NM,CS}} E_{\mathbf{PR}_{\mathrm{GW}}, \mathbf{PR}_{\mathrm{OVN}}\mid \mathbf{PR}_{\mathrm{VDZ}}, \mathbf{NM,CS}} \left(\mathbf{\Delta} \mid \mathbf{PR}_{\mathrm{VDZ}}, \mathbf{NM, CS}\right)}{V(\mathbf{\Delta})} = \frac{V(\mathbf{PR}_{\mathrm{VDZ}})}{V(\mathbf{\Delta})}, \tag{11}
$$

https://doi.org/10.5194/hess-2020-87
Preprint. Discussion started: 10 March 2020

Hydrology and Earth System Sciences
Discussions

$$S_{\mathbf{PR}_{\mathrm{GW}}} = \frac{E_{\mathbf{CS}} E_{\mathbf{NM|CS}} V_{\mathbf{PR}_{\mathrm{GW}}|\mathbf{NM},\mathbf{CS}} E_{\mathbf{PR}_{\mathrm{VDZ}},\mathbf{PR}_{\mathrm{OVN}}|\mathbf{PR}_{\mathrm{GW}},\mathbf{NM},\mathbf{CS}} \left(\boldsymbol{\Delta} \mid \mathbf{PR}_{\mathrm{GW}}, \mathbf{NM}, \mathbf{CS}\right)}{V\left(\boldsymbol{\Delta}\right)} = \frac{V\left(\mathbf{PR}_{\mathrm{GW}}\right)}{V\left(\boldsymbol{\Delta}\right)}, \tag{12}$$

$$S_{\mathbf{PR}_{\mathrm{OVN}}} = \frac{E_{\mathbf{CS}} E_{\mathbf{NM|CS}} V_{\mathbf{PR}_{\mathrm{OVN}}|\mathbf{NM},\mathbf{CS}} E_{\mathbf{PR}_{\mathrm{VDZ}},\mathbf{PR}_{\mathrm{GW}}|\mathbf{PR}_{\mathrm{OVN}},\mathbf{NM},\mathbf{CS}} \left(\boldsymbol{\Delta} \mid \mathbf{PR}_{\mathrm{OVN}}, \mathbf{NM}, \mathbf{CS}\right)}{V\left(\boldsymbol{\Delta}\right)} = \frac{V\left(\mathbf{PR}_{\mathrm{OVN}}\right)}{V\left(\boldsymbol{\Delta}\right)}. \tag{13}$$

2.3 Sensitivity index estimation using the Latin hypercube sampling and binning method

In this study, the parameters were sampled with a sample size of 600 within the feasible range via Latin hypercube sampling (LHS) (Kanso et al., 2006; Zhang and Pinder, 2003). LHS is a type of constrained Monte Carlo sampling that can accurately reflect the function distribution of the input data. Compared with Monte Carlo sampling, LHS greatly reduces the demand for sample size and computation time and is widely used in modeling simulation and optimization calculations. For the function $\mathbf{Y} = f\left(\mathbf{X}\right)$, where $\mathbf{X} = \left\{X_1, X_2, ..., X_3\right\}$, by using LHS, the range of X_i, $i = 1, 2, ..., k$ can be divided into n non-overlapping intervals with equal probabilities. The n values obtained from X_1 are randomly paired with n values obtained from X_2; these n paired values are then combined with those n values from X_3. We repeat this process until the new $n \times k$ matrix, $\mathbf{X}$, is developed. The sample matrix $\mathbf{X}$ can be used to calculate the sensitivity index for the model output. More details regarding LHS are described in previous studies (McKay, 1979; Owen, 1998; Helton, 2003).

Using the variance definition, the partial variance of V(**PR**) can be expressed as:

$$\begin{aligned} V\left(\mathbf{PR}\right) &= E_{\mathbf{CS}} E_{\mathbf{NM|CS}} V_{\mathbf{PR|NM,CS}} \left(\boldsymbol{\Delta} \mid \mathbf{NM}, \mathbf{CS}\right) \\ &= E_{\mathbf{CS}} E_{\mathbf{NM|CS}} \left(E_{\mathbf{PR|NM,CS}} \left(\boldsymbol{\Delta} \mid \mathbf{NM}, \mathbf{CS}\right)^2 - \left(E_{\mathbf{PR|NM,CS}} \left(\boldsymbol{\Delta} \mid \mathbf{NM}, \mathbf{CS}\right)\right)^2\right). \end{aligned} \tag{14}$$

In this study, there are l=6 alternative climate scenarios, and under each climate scenario, there are k=3 plausible models, and we have n=600 sampled parameter sets for each model and climate scenario. After applying the formula of expectation and the LHS method, the terms of $V\left(\mathbf{PR}\right)$, $V\left(\mathbf{NM}\right)$ and $V\left(\mathbf{CS}\right)$ can be expressed as:

$$\begin{aligned} V\left(\mathbf{PR}\right) &= E_{\mathbf{CS}} E_{\mathbf{NM|CS}} \left(E_{\mathbf{PR|NM,CS}} \left(\boldsymbol{\Delta} \mid \mathbf{NM}, \mathbf{CS}\right)^2 - \left(E_{\mathbf{PR|NM,CS}} \left(\boldsymbol{\Delta} \mid \mathbf{NM}, \mathbf{CS}\right)\right)^2\right) \\ &= E_{\mathbf{CS}} E_{\mathbf{NM|CS}} \left(\frac{1}{n}\sum_{j=1}^{n} \Delta^2\left(PR_j \mid NM_k, CS_l\right) - \left(\frac{1}{n}\sum_{j=1}^{n} \Delta\left(PR_j \mid NM_k, CS_l\right)\right)^2\right) \\ &= \sum_l \sum_k \left(\frac{1}{n}\sum_{j=1}^{n} \Delta^2\left(PR_j \mid NM_k, CS_l\right) - \left(\frac{1}{n}\sum_{j=1}^{n} \Delta\left(PR_j \mid NM_k, CS_l\right)\right)^2\right) P\left(NM_k \mid CS_l\right) P\left(CS_l\right) \end{aligned}, \tag{15}$$

https://doi.org/10.5194/hess-2020-87
Preprint. Discussion started: 10 March 2020


Hydrology and Earth System Sciences
Discussions

$$V(\mathbf{NM}) = E_{\mathbf{CS}} V_{\mathbf{NM}|\mathbf{CS}} E_{\mathbf{PR}|\mathbf{NM},\mathbf{CS}}(\boldsymbol{\Delta}\,|\,\mathbf{NM},\mathbf{CS})$$
$$= \sum_l P(CS_l)\left(\begin{array}{l}\sum_k \left(\frac{1}{n}\sum_{j=1}^{n}\Delta(PR_j \mid NM_k, CS_l)\right)^2 P(NM_k \mid CS_l) - \\ \left(\sum_k \left(\frac{1}{n}\sum_{j=1}^{n}\Delta(PR_j \mid NM_k, CS_l) P(NM_k \mid CS_l)\right)\right)^2\end{array}\right), \quad (16)$$

$$V(\mathbf{CS}) = V_{\mathbf{CS}} E_{\mathbf{NM},\mathbf{CS}} E_{\mathbf{PR}|\mathbf{NM},\mathbf{CS}}(\Delta\,|\,\mathbf{NM},\mathbf{CS})$$
$$= \sum_l P(CS_l)\left(P(NM_k \mid CS_l)\left(\frac{1}{n}\sum_{j=1}^{n}\Delta_k(PR_j \mid NM_k, CS_l)\right)\right)^2 \quad , \quad (17)$$
$$-\left(\sum_l \sum_k P(CS_l) P(NM_k \mid CS_l)\left(\frac{1}{n}\sum_{j=1}^{n}\Delta_k(PR_j \mid NM_k, CS_l)\right)\right)^2$$

where n and j represent the parameter LHS sample number and index, respectively, $P(NM_k|CS_l)$ represents the weight of model NM_k under climate scenario CS_l with $\sum_k P(NM_k|CS_l)=1$, and $P(CS_l)$ is the weights of different climate scenario situations satisfying $\sum_l P(CS_l)=1$. The values of the weights for alternative models or climate scenarios could be selected using prior knowledge or objective criteria, e.g., posterior probabilities of the Bayesian theorem (Neumann, 2012; Schoniger et al., 2014).

To calculate the subdivided parametric sensitivity indices, i.e., the sensitivity indices for vadose zone parameters, groundwater parameters, and the overland flow parameter, a binning method was implemented in this study. The main concept of the binning method is to approximate the mean value for a single parameter by substituting the mean value for this parameter in a bin. Taking the sensitivity index of vadose zone parameters as an example, since $E_{\mathbf{PR}_{\mathrm{VDZ}}|\mathbf{NM},\mathbf{CS}}(\Delta|\mathbf{PR}_{\mathrm{VDZ}},\mathbf{NM},\mathbf{CS}) = \sum E_{\mathbf{PR}^{\mathrm{bin}}_{\mathrm{VDZ}}|\mathbf{NM},\mathbf{CS}}$, the term $E_{\mathbf{PR}_{\mathrm{GW}},\mathbf{PR}_{\mathrm{OVN}}|\mathbf{PR}_{\mathrm{VDZ}},\mathbf{NM},\mathbf{CS}}(\Delta|\mathbf{PR}_{\mathrm{VDZ}},\mathbf{NM},\mathbf{CS})$ in Eq. (11) can be computed as $E_{\mathbf{PR}_{\mathrm{GW}},\mathbf{PR}_{\mathrm{OVN}}|\mathbf{PR}_{\mathrm{VDZ}},\mathbf{NM},\mathbf{CS}}(\Delta|\mathbf{PR}^{\mathrm{bin}}_{\mathrm{VDZ}},\mathbf{NM},\mathbf{CS})$. The procedures for calculating the subdivided parametric sensitivity indices for $\mathbf{PR}_{\mathrm{VDZ}}$ using the combined LHS and binning methods are as follows: (1) simulate Δ for all climate scenarios, numerical models, and parameter realizations, (2) divide the $\mathbf{PR}_{\mathrm{VDZ}}$ realizations into bins, and (3) calculate $E_{\mathbf{PR}_{\mathrm{GW}},\mathbf{PR}_{\mathrm{OVN}}|\mathbf{PR}_{\mathrm{VDZ}},\mathbf{NM},\mathbf{CS}}(\Delta|\mathbf{PR}_{\mathrm{VDZ}},\mathbf{NM},\mathbf{CS})$ by replacing it with $E_{\mathbf{PR}_{\mathrm{GW}},\mathbf{PR}_{\mathrm{OVN}}|\mathbf{PR}_{\mathrm{VDZ}},\mathbf{NM},\mathbf{CS}}(\Delta|\mathbf{PR}^{\mathrm{bin}}_{\mathrm{VDZ}},\mathbf{NM},\mathbf{CS})$. After $E_{\mathbf{PR}_{\mathrm{GW}},\mathbf{PR}_{\mathrm{OVN}}|\mathbf{PR}_{\mathrm{VDZ}},\mathbf{NM},\mathbf{CS}}(\Delta|\mathbf{PR}^{\mathrm{bin}}_{\mathrm{VDZ}},\mathbf{NM},\mathbf{CS})$ is calculated for each bin of $\mathbf{PR}_{\mathrm{VDZ}}$, the sensitivity index for $\mathbf{PR}_{\mathrm{VDZ}}$ of Eq. (11) can be expressed as:

$$S_{\mathbf{PR}_{\mathrm{VDZ}}} = \frac{E_{\mathbf{CS}} E_{\mathbf{NM}|\mathbf{CS}} V_{\mathbf{PR}^{\mathrm{bin}}_{\mathrm{VDZ}}|\mathbf{NM},\mathbf{CS}} E_{\mathbf{PR}_{\mathrm{GW}},\mathbf{PR}_{\mathrm{OVN}}|\mathbf{PR}^{\mathrm{bin}}_{\mathrm{VDZ}},\mathbf{NM},\mathbf{CS}}(\boldsymbol{\Delta}\,|\,\mathbf{PR}^{\mathrm{bin}}_{\mathrm{VDZ}},\mathbf{NM},\mathbf{CS})}{V(\boldsymbol{\Delta})} = \frac{V(\mathbf{PR}_{\mathrm{VDZ}})}{V(\boldsymbol{\Delta})}. \quad (18)$$

https://doi.org/10.5194/hess-2020-87
Preprint. Discussion started: 10 March 2020


Hydrology and Earth System Sciences
Discussions

where the subscript $\mathbf{PR}_{VDZ}^{bin}|\mathbf{NM}$, **CS** represents the change in the bins for vadose zone parameters under a fixed numerical model and a fixed climate scenario. The subscript $\mathbf{PR}_{GW}$, $\mathbf{PR}_{OVN}|\mathbf{PR}_{VDZ}^{bin}$, **NM**, **CS** represents the change in the $\mathbf{PR}_{GW}$ and $\mathbf{PR}_{OVN}$ sets belonging to a specific $\mathbf{PR}_{VDZ}$ bin under a fixed numerical model and a fixed climate scenario.

Moreover, the sensitivity indices for $\mathbf{PR}_{GW}$ and $\mathbf{PR}_{OVN}$ can be estimated as:

$$S_{\mathbf{PR}_{GW}} = \frac{E_{\mathbf{CS}} E_{\mathbf{NM}|\mathbf{CS}} V_{\mathbf{PR}_{GW}^{bin}|\mathbf{NM},\mathbf{CS}} E_{\mathbf{PR}_{VDZ},\mathbf{PR}_{OVN}|\mathbf{PR}_{GW}^{bin},\mathbf{NM},\mathbf{CS}} \left(\boldsymbol{\Delta} \mid \mathbf{PR}_{GW}^{bin}, \mathbf{NM}, \mathbf{CS}\right)}{V(\boldsymbol{\Delta})} = \frac{V(\mathbf{PR}_{GW})}{V(\boldsymbol{\Delta})}, \quad (19)$$

$$S_{\mathbf{PR}_{OVN}} = \frac{E_{\mathbf{CS}} E_{\mathbf{NM}|\mathbf{CS}} V_{\mathbf{PR}_{OVN}^{bin}|\mathbf{NM},\mathbf{CS}} E_{\mathbf{PR}_{VDZ},\mathbf{PR}_{GW}|\mathbf{PR}_{OVN}^{bin},\mathbf{NM},\mathbf{CS}} \left(\boldsymbol{\Delta} \mid \mathbf{PR}_{OVN}^{bin}, \mathbf{NM}, \mathbf{CS}\right)}{V(\boldsymbol{\Delta})} = \frac{V(\mathbf{PR}_{OVN})}{V(\boldsymbol{\Delta})}. \quad (20)$$

Using LHS and the binning method, the number of realizations is reduced to the size of the parameter sets obtained from the LHS method. Thus, the computation cost for estimating the subdivided parametric indices can be highly reduced. In this case, the sample size of $\mathbf{PR}_{VDZ}$ is 600, and the number of possible combinations of $\mathbf{PR}_{GW}$ and $\mathbf{PR}_{OVN}$ is $600\times600/2=180{,}000$; then, the number of realizations of regular Monte Carlo simulations is $600\times180{,}000=1.08\times10^{8}$. Using LHS and the binning method, the number of realizations is reduced to 180,000. Dai et al. (2017b) confirmed a similar accuracy of 36,000,000 Monte Carlo realization results with 16,000 realizations when applying only the binning method for a synthetic example. The combination of the LHS method with the binning method makes it possible to further reduce the computational cost for such a large-scale, complex hydrologic model.

2.4 Uncertainty sources and the generation of uncertain inputs

In this study, climate scenarios, model structures, and parameters are treated as random uncertain inputs or uncertainty sources to assess the sensitivity for two model outputs of interest: evapotranspiration (*ET*) and groundwater contribution to streamflow (Q_G). For the climate scenarios, we generated six typical and alternative scenarios based on NASA's Tropical Measuring Mission (TRMM) data (http://trmm.gsfc.nasa.gov/) and the default CLM CRU-NCEP (CRUNCEP) dataset (Piao et al., 2012) from 1998 to 2013. The precipitation data were obtained from the TRMM while the temperature, solar radiation, humidity and wind speed data are based on the CRUNCEP because the model fails to capture the peak stream discharges using the CRUNCEP rainfall data (Niu et al., 2017). We first divided the full climate dataset into dry and wet seasons according to the precipitation values (six months for each season). Then, we sorted the different seasons according to their total precipitation values during the whole season. Next, we divided these wet and dry seasons into three different groups representing six climate scenarios from wet to dry (Fig. 3). The mean and standard deviation of the values of the different climate variables (e.g., precipitation, maximum temperature) for each group were calculated using the daily data (Table 1). Finally, we generated random daily weather data for each climate scenario based on these mean and standard deviation data using a normal distribution. The mean and standard deviation for each climate scenario's daily data are listed in Table 1, and

https://doi.org/10.5194/hess-2020-87
Preprint. Discussion started: 10 March 2020


Hydrology and Earth System Sciences
Discussions

Fig. 3 displays a box plot of the precipitation data for the six climate scenarios (CS_1, CS_2, CS_3, CS_4, CS_5, CS_6). In this study, we assumed that the different scenarios have equal probability. However, we changed the probabilities for CS_1 (the wettest climate scenario) and CS_6 (the driest climate scenario) in Section 3.5 to investigate the influences of extreme climate scenarios on the sensitivity analysis results.

According to Pelletier et al. (2016), the thickness of the unconfined aquifer in the central Amazon is larger than 50 m, and the depth of the bedrock is very deep. Niu et al. (2017) simulated an unconfined aquifer with 100 m depth and 200 m thickness for the confined aquifer. In this study, we wanted to investigate the sensitivity of the model outputs to aquifer thickness, so we generated three aquifer models involving different thicknesses of the unconfined and confined aquifers: (1) 100 m and 200 m (NM_1), (2) 50 m and 250 m (NM_2), and (3) 250 m and 50 m (NM_3), respectively. These three aquifer models were assumed to have equal weights (probabilities), but changes in these probabilities were also investigated in Section 3.5.

We adjusted the values of six model parameters and classified them into three groups to explore the parametric sensitivities. The first group includes vadose zone parameters (PR_{VDZ}): the Van Genuchten soil parameters α and N and soil saturated conductivity, K_s. The second group is composed of groundwater parameters (PR_{GW}): unconfined aquifer conductivity, K_1, and confined aquifer conductivity, K_2. The third group is the overland flow parameter (PR_{OVN}): length of the flow path for runoff contribution to the overland flow domain, L. The allowable ranges of these six parameters are listed in Table 2. To ensure that the sensitivity analysis was uncomplicated and computationally tractable, each grid was given the same value for a specific parameter.

The soil saturated conductivity, K_s (m day^{-1}), unconfined aquifer conductivity, K_1 (m day^{-1}), and confined aquifer conductivity, K_2 (m day^{-1}), were assumed to follow lognormal distributions (log-N (1.6094, 0.4214^2), log-N (3.4012, 0.4214^2), and log-N (1.6094, 0.4214^2), respectively). The remaining three parameters (α, N, and L) were assumed to follow a uniform distribution: U (0.1, 4), U (1.03, 5), and U (20, 700), respectively.

3 Results and discussion

3.1 Model predictions

The total number of PAWS+CLM simulations considering all possible combinations of the three uncertain factors is 6×3×600=10,800, which represents six climate scenarios, three model conceptualizations of aquifer thickness, and 600 sampled parameter sets. In this study, we first used equal weights for the climate scenarios and numerical models, i.e., $P(CS_l)=\frac{1}{6}$ and $P(NM_k|CS_l)=\frac{1}{3}$. In Section 3.5, we investigated the influences of different prior probabilities for the climate scenarios and numerical models. The simulation time for all the simulations was six months (180 days, 4320 hours), which is the length of the dry or wet season in the central Amazon region. The results given by PAWS were represented in two forms: (1) space-averaged output values over the whole grid at each time step; (2) time-averaged output values over the whole simulated period for each grid. In this study, the time step is one hour. Figure 4 depicts the spatially averaged model

https://doi.org/10.5194/hess-2020-87
Preprint. Discussion started: 10 March 2020


Hydrology and Earth System Sciences
Discussions

predictions at the simulation time of 2868 hours (wall-clock time: 12:00) for the two outputs of interest, *ET* and Q_G, with different inputs of scenarios, models, and parameter sets. The results demonstrate the large variabilities or uncertainties among the predictions of the different model realizations, and these uncertainties were contributed by all three sources of uncertainty: scenarios, models, and parameters. Further accurate sensitivity analysis is capable of identifying the most important sources of uncertainty.

3.2 Sensitivity indices for evapotranspiration

We first calculated the sensitivity indices for the spatially averaged *ET* over the whole watershed at all time steps using Eqs. (5)-(7). Figure 5(a) shows the sensitivity indices for the whole simulation period of 4320 time steps. All the sensitivity indices fluctuate strongly with time, except for the numerical models. The sensitivity indices for the numerical models ($S_{\mathbf{NM}}$) are always close to zero at every time step, indicating that aquifer thickness has little influence on *ET*. Figures 5(b)-(g) plot the sensitivity indices across six periods, exhibiting the details at each time step. Every period lasts for three days. It seems that the patterns of the sensitivity indices have a daily cycle, but specific values of the sensitivity indices at the same wall-clock time on different days are distinguished. Figure 5 indicates that the sensitivity to various factors is strongly temporally dependent. However, it should be noted that at the wall-clock time of 12:00-13:00, the climate scenarios are always the most important factors affecting the sensitivity of *ET* because *ET* is directly influenced by solar radiation values, and the radiation forcing used in this study reaches its maximum value at approximately 12:00. At the wall-clock time of 24:00-1:00, the sensitivity indices for the parameters ($S_{\mathbf{PR}}$) show absolute dominance since precipitation and radiation forcing all decrease to zero, leading to the differences in rainfall and radiation among the climate scenarios greatly decreasing.

Six time points (simulation times = 1428 hour, 1440 hour, 2868 hour, 2880 hour, 4308 hour, and 4320 hour) were chosen as examples to show the sensitivity indices (Fig. 6). Simulation times of 1428 hour, 2868 hour, and 4320 hour belonged to different days but all corresponded to 12:00 local time. At these time points, the climate scenario uncertainty ($S_{\mathbf{CS}}$) is the most important contributor to the total *ET* prediction uncertainty, accounting for 54-77% of the total uncertainty, and parameters ($S_{\mathbf{PR}}$) contribute the second most to uncertainty. However, at different time points (1440 hour, 2880 hour, and 4320 hour, corresponding to 24:00 local time), the parameters are the dominant uncertainty contributor, with $S_{\mathbf{PR}}$ ranging from 89 to 92%. We also calculated the sensitivity indices for every grid cell within the model domain using the time-averaged *ET* predictions over all simulation periods (4320 hours). Figure 7 shows the spatial variability of the sensitivity indices for the temporal mean *ET* predictions. The maps demonstrate that for most grids, parameters are the most important uncertainty contributor to *ET* predictions ($S_{\mathbf{PR}}$>0.50), and climate scenarios are the second most important contributor to uncertainty. However, for the stream grid cells, the importance of model uncertainty increases. The parameters and aquifer thickness are both important for the *ET* predictions in river grid cells. This sensitivity occurs because the aquifer thickness along the streams will affect the exchange between the groundwater cells and the river cells (the relevant process is shown in Appendix A).

https://doi.org/10.5194/hess-2020-87
Preprint. Discussion started: 10 March 2020


Hydrology and Earth System Sciences
Discussions

3.3 Sensitivity indices for groundwater contribution to streamflow

The same sensitivity analysis procedures were also conducted for the model predictions of Q_G. Groundwater is an important component of hydrologic processes in the central Amazon region; therefore, it is essential to conduct sensitivity analysis for Q_G. Figure 8(a) shows that regardless of the time step, parameters are always the dominant contributor to the total Q_G prediction uncertainty because soil parameters strongly affect the soil water redistribution process, including the infiltration into groundwater. The sensitivity indices of the models ($S_{\mathbf{NM}}$) and climate scenarios ($S_{\mathbf{CS}}$) reach peak values at approximately 1:00 (Figs. 8(b)-(g)). This may be because the exchange between groundwater and river flow always occurs hours later than the rainfall process, and the value of the exchange process always reaches its peak at night, at approximately 1:00. Furthermore, the thickness of an aquifer will greatly influence the water redistribution process in the aquifer. It should be noted that, in Fig. 8(a), the values of the sensitivity indices for the climate scenarios are cumulative. In the beginning, the importance of the climate scenarios is negligible, but over time, the importance of the climate scenarios increases. This pattern can be explained by the fact that the climate scenarios have no immediate direct influence on groundwater flow $S_{\mathbf{NM}}$, but over time, the amount of groundwater in aquifers will be affected, and this influence is long-term and cumulative. Because groundwater exchange with stream flow occurs only at grid cells along the streams, the sensitivity indices only have valid values in those stream grid cells (Fig. 9). Our results indicate that for most stream grid cells, the parameters are the most important contributor to the total uncertainty of time-averaged Q_G predictions. The second most important factor is aquifer thickness.

3.4 Sensitivity indices for subdivided parameters

Based on the sensitivity analysis for *ET* and Q_G, the results show that parameters are the most important uncertain input for both the spatially averaged and time-averaged uncertainties. In this study, we used Eqs. (11)-(13) to further calculate the subdivided parametric sensitivity indices, which can provide more detailed sensitivity analysis for model simulation. Through this investigation, the parametric sensitivity was subdivided into three groups: (1) the sensitivity for vadose zone parameters ($\mathbf{PR}_{VDZ}$), (2) the sensitivity for groundwater parameters ($\mathbf{PR}_{GW}$), and (3) the sensitivity for the overland flow parameter ($\mathbf{PR}_{OVN}$). Using the binning method, we calculated the spatially averaged and time-averaged subdivided parametric sensitivity indices for *ET* and Q_G. We plotted frequency histograms of the subdivided parametric sensitivity indices over 4320 hours in Fig. 10.

Figure 10(a) depicts the results for *ET*. The value of $S_{\mathbf{PR}_{VDZ}}$ is concentrated in the range of 0.1-0.9, and $S_{\mathbf{PR}_{GW}}$ is concentrated in the range of 0.003-0.032. The value of $S_{\mathbf{PR}_{OVN}}$ is so small that the influence of the overland flow parameter can be ignored. This indicates that vadose zone parameters ($\mathbf{PR}_{VDZ}$) dominate the total parametric uncertainties for *ET*. Figure 10(b) shows the frequency histogram of spatially averaged subdivided parametric sensitivity results for Q_G. $S_{\mathbf{PR}_{VDZ}}$ is still concentrated in

https://doi.org/10.5194/hess-2020-87
Preprint. Discussion started: 10 March 2020


Hydrology and Earth System Sciences
Discussions

the larger number range (0.2-0.53), and the value of $S_{\mathbf{PR}_{GW}}$ changes from 0.04 to 0.3. The number of $S_{\mathbf{PR}_{OVN}}$ is also the lowest, indicating that the overland flow parameter has little effect on Q_G.

We plotted the time-averaged subdivided parametric sensitivity indices for *ET* in Fig. 11(a) and for Q_G in Fig. 11(b). Considering *ET* as our output, for most grids, the vadose zone parameters are the most important contributor to parametric uncertainties. Compared with that on other grids, the influence of groundwater parameters on the river grids is more significant (Fig. 11(a)). In terms of Q_G, for most grids, the vadose zone parameters dominate the parametric sensitivities (Fig. 11(b)). For both time-averaged *ET* and Q_G, the impact of the overland flow parameter can be ignored.

3.5 Effects of prior weights on sensitivity indices

In this section, we changed the prior weights of the climate scenarios and numerical models to investigate their influences on the space-averaged sensitivity indices. Because the number of space-averaged results for *ET* and Q_G is too large to be well exhibited, we chose one time step (4308 hour, 12:00 wall-clock time) to show the trend. We randomly changed the values of the prior weights for NM_1 (the thickness of the unconfined aquifer is 50 m, and that of the confined aquifer is 250 m), CS_1 (the wettest climate scenario), and CS_6 (the driest climate scenario) to between 0 and 1. The values of these factors' prior weights were randomly changed. Figure 12(a) indicates that when we consider *ET* as our output, with the increase in the prior weight of NM_1, the uncertainty of the climate scenarios will decrease to 50%, while the uncertainty of the parameters will increase to 50%. Both parameters and climate scenarios have quite important effects on *ET*. Different from the results for *ET*, with the increase in the prior weights of NM_1, the sensitivity index of the numerical models for Q_G decreases to 0 (because only one model exists under this condition), and the scenario uncertainty changes only slightly. Moreover, the uncertainty of parameters always dominates the total uncertainty for Q_G (Fig. 12(b)) regardless of the prior weight value. In general, the different prior weight values for the numerical models only slightly change the sensitivity analysis results.

Figures 12(c)-(f) exhibit the influences of prior weights for the wettest and the driest climate scenarios on *ET*. These figures first demonstrate that changing the values of the prior weights of CS_1 and CS_6 have larger impacts on *ET* predictions than on Q_G predictions. This pattern coincides with the fact that the parameter uncertainty dominates the total predictive uncertainty of Q_G and that the scenario uncertainty is relatively small. Therefore, the selection of prior weight values for the scenarios does not have a significant effect on the sensitivity analysis results for the Q_G predictions, and the parameter sensitivity index is always the largest (Fig. 12(d) and (f)). For the sensitivity analysis results pertaining to *ET* predictions, changing the values of the weights for CS_1 and CS_6 has different effects. The sensitivity index values of the climate scenarios for *ET* predictions monotonically decrease while the importance of parameters continues to increase as the prior weight of CS_1 rises. However, the value of $S_{\mathbf{CS}}$ for *ET* predictions first increases and then dramatically decreases after the prior weight of CS_6 approaches 80%, and $S_{\mathbf{PR}}$ shows the opposite trend (Fig. 12(e)). The different effects on *ET* predictions of CS_1 and CS_6 might be caused by their distinct temperatures and radiation intensities.

https://doi.org/10.5194/hess-2020-87
Preprint. Discussion started: 10 March 2020


Hydrology and Earth System Sciences
Discussions

4 Conclusions

In this study, we implemented an advanced hierarchical sensitivity analysis method and a complex large-scale process-based hydrological model (PAWS) to identify important uncertain inputs for *ET* and Q_G predictions in an Amazonian watershed. This sensitivity analysis method is capable of providing accurate measurements of the importance of uncertain inputs through variance decomposition, and it can also categorize and combine different uncertain inputs considering their dependence relationships to decrease the high dimensionality induced by a complex and large-scale problem. Three groups of uncertainty sources or uncertain inputs were considered in this study, including six climate scenarios, three plausible aquifer models, and six uncertain parameters (i.e., soil saturated conductivity, Van Genuchten α and N, unconfined aquifer conductivity, confined aquifer conductivity, and the length of the flow path for runoff contribution to the overland flow domain). A new set of subdivided parametric sensitivity indices was defined for three groups of parametric uncertainty sources (i.e., vadose zone, groundwater, and overland flow parameters). When researchers use this hierarchical sensitivity analysis method, and there are some processes at a certain layer that can be further separated, this study provides a feasible way to investigate more detailed information for the grouped uncertainties. The implementation of the Latin hypercube sampling method and the binning method reduced the high computational cost.

The sensitivity analysis results in this study demonstrate that parameter uncertainty is important in both time-averaged and space-averaged predictions regardless of whether the output is evapotranspiration or groundwater contribution to streamflow. Among all the parameter uncertainties, the vadose zone parameters are the most important, and the parameter of overland flow is negligible. The climate scenarios are also important uncertainties in evapotranspiration predictions, especially at the wall-clock time of 12:00 noon. Along the river grid cells, the thickness of the aquifer has a non-ignorable influence on both evapotranspiration and groundwater contribution to streamflow. On the basis of the results of this study, we suggest that when modelers use sophisticated hydrological simulators such as PAWS, they should pay attention to the weather variable values at approximately 12:00 noon (always the daily peak values), investigate the thickness of groundwater aquifers near rivers and adjust the parameters of the vadose zone.

This study represents a pilot example of comprehensive global sensitivity analysis considering all uncertainty sources in a large-scale hydrological model. The sensitivity analysis results can provide key information on uncertainty sources for modelers and greatly improve the model calibration and uncertainty analysis processes. By categorizing multiple uncertainties into processes and placing them into a proper layer in a hierarchical framework, this advanced hierarchical sensitivity analysis method can largely reduce the computational cost associated with complex, large-scale hydrological models. Its combination with Latin hypercube sampling and the binning method can further decrease the computational cost. The proposed method is mathematically rigorous and general and can be applied to extensive, large-scale hydrological or environmental models with more or different sources of uncertainty.

https://doi.org/10.5194/hess-2020-87
Preprint. Discussion started: 10 March 2020

Hydrology and Earth System Sciences
Discussions

Acknowledgments

This work was supported by the National Natural Science Foundation of China (41807182).

Appendix A

The governing equations of PAWS are presented in detail in Shen and Phanikumar (2010) and Shen et al. (2013). Here, we will mainly introduce the equations describing the processes involved in this article.

In PAWS, the moisture of the soil in the vadose zone is calculated according to the Richards equation. The vertical movement of fluid between saturated and unsaturated soil is calculated on the basis of the mixed form of the Richards equation (Celia et al., 1990; van Dam and Feddes, 2000):

$$C(h)\frac{\partial h}{\partial t}=\frac{\partial}{\partial z}\left[K(h)\left(\frac{\partial h}{\partial z}+1\right)\right]+W(h)\,. \tag{A.1}$$

where h represents the soil water pressure head, z is the elevation (positive upward), $K(h)$ represents the soil unsaturated conductivity and $W(h)$ is the source or sink term, including the influence of evaporation, root extraction and lateral flow. The differential water capacity can be described as $C(h)=\partial\theta/\partial h$, where h is the soil pressure head and θ is the water content. The pressure head, h, is related to the unsaturated hydraulic conductivity, $K(h)$. According to the Mualem-van Genuchten formula (Mualem, 1976; van Genuchten,1980), the soil saturated hydraulic conductivity, K_s, Van Genuchten α and N will influence the unsaturated conductivity, $K(h)$:

$$S=\frac{\theta(h)-\theta_r}{\theta_s-\theta_r}=\left(1+\left|\alpha h\right|^N\right)^{-(N-1)/N}, \tag{A.2}$$

$$K(h)=K_s S^{\lambda}\left[1-\left(1-S^{N/(N-1)}\right)^{(N-1)/N}\right]^2, \tag{A.3}$$

where S is the relative saturation, θ_s is the saturated water content, θ_r is the residual water content, N is related to the pore-size distribution, α indicates the reciprocal of air suction and λ is a parameter measuring pore connectivity.

The aquifers in PAWS are depicted as a series of 2-D layers (Shen et al., 2014). In each layer, the 2-D groundwater equation is used to describe the water movement:

$$S\frac{\partial H}{\partial t}=\frac{\partial}{\partial x}\left[T\left(\frac{\partial H}{\partial x}\right)\right]+\frac{\partial}{\partial y}\left[T\left(\frac{\partial H}{\partial y}\right)\right]+R+W-Dp\,, \tag{A.4}$$

https://doi.org/10.5194/hess-2020-87
Preprint. Discussion started: 10 March 2020


Hydrology and Earth System Sciences
Discussions

where S is the storability; T is the transmissivity of the aquifer; $T=Kb$, where K is the aquifer conductivity and b is the saturated thickness of the aquifer; H is the aquifer hydraulic head; R is recharge or discharge; W is the source and sink term; and Dp is percolation into deeper aquifers.

PAWS applies one-dimensional diffusive wave equations to portray the channel flow model (Shen and Phanikumar, 2010; Shen et al., 2014). After calculating the channel flow, the exchange between groundwater and channel flow (Q_G) is immediately computed. The calculation of Q_G is based on the leakance concept (Shen and Phanikumar, 2010):

$$\frac{h_r^{n+1} - h_r^*}{\Delta t} = K_r \frac{H^* - (Z_b + h_r^{n+1})}{\Delta Z_b}, \tag{A.5}$$

where h_r^* is the river level calculated from the channel flow model, K_r is the riverbed conductivity, Z_b is the elevation of river bed, ΔZ_b is the thickness of the riverbed and H^* is the groundwater table. Note that H^* can also be described as Eq. (A.5). By solving these two equations together, we can obtain H^* and h_r^{n+1}. Then, the value of Q_G can be calculated as (Shen and Phanikumar, 2010):

$$Q_G = w\left(h_r^{n+1} - h_r^*\right), \tag{A.6}$$

where w is the wetted perimeter. If the river width is greater than 10 m, w can be approximated as the river width.

PAWS retains its own flow scheme, but the surface processes use the CLM 4.0 model. This enables the simulation of detailed surface processes such as surface heat flux, water vapor flux, surface radiation balance, crop growth, and plant photosynthesis. The calculation of *ET* demand is performed in the CLM model based on the climate data, and then *ET* demand will be transferred to PAWS as a source term for the vadose zone. More details about the calculation of *ET* (both evaporation and transpiration information can be found in the technical note of CLM 4.0, http://www.cesm.ucar.edu/models/cesm1.1/clm/CLM4_Tech_Note.pdf). The coupling with the CLM makes PAWS a more comprehensive and robust surface-subsurface hydrological model.

References

Baroni, G., and Tarantola, S.: A General Probabilistic Framework for uncertainty and global sensitivity analysis of deterministic models: A hydrological case study, Environ Modell Softw, 51, 26-34, 2014.

Beighley, R. E., Eggert, K. G., Dunne, T., He, Y., Gummadi, V., and Verdin, K. L.: Simulating hydrologic and hydraulic processes throughout the Amazon River Basin, Hydrol Process, 23, 1221-1235, 2009.

Beven, K. J.: Towards an alternative blueprint for a physically based digitally simulated hydrologic response modelling system, Hydrol. Process. 16, 189–206. doi:10.1002/hyp.343, 2002.

Celia, M. A., Bouloutas, E. T., and Zarba, R. L.: A general mass-conservative numerical solution for the unsaturated flow equation, Water Resour Res, 26, 1990.

Chavarri, E., Crave, A., Bonnet, M. P., Mejia, A., Da Silva, J. S., and Guyot, J. L.: Hydrodynamic modelling of the Amazon River: Factors of uncertainty, J S Am Earth Sci, 44, 94-103, 2013.

Coe M. T., Costa M. H., and Howard E. A.: Simulating the surface waters of the Amazon River basin: impacts of new river geomorphic and flow parameterizations, Hydrol Process, 22, 2542-2553, doi:10.1002/hyp.6850, 2008.

Dai, H., and Ye, M.: Variance-based global sensitivity analysis for multiple scenarios and models with implementation using sparse grid collocation, J Hydrol, 528, 286-300, 2015.

Dai, H., Chen, X., Ye, M., Song, X., and Zachara, J. M.: A geostatistics-informed hierarchical sensitivity analysis method for complex groundwater flow and transport modeling, Water Resour Res, 53, 2017a.

Dai, H., Ming, Y., Walker, A. P., and Chen, X.: A new process sensitivity index to identify important system processes under process model and parametric uncertainty, Water Resour Res, 53, 3476-3490, 2017b.

de Paiva, R. C. D., Buarque, D. C., Collischonn, W., Bonnet, M. P., Frappart, F., Calmant, S., and Mendes, C. A. B.: Large-scale hydrologic and hydrodynamic modeling of the Amazon River basin, Water Resour Res, 49, 1226-1243, 2013.

Draper, D., Pereira, A., Prado, P., Saltelli, A., Cheal, R., Eguilior, S., Mendes, B., and Tarantola, S.: Scenario and parametric uncertainty in GESAMAC: A methodological study in nuclear waste disposal risk assessment, Comput Phys Commun, 117, 142-155, https://doi.org/10.1016/S0010-4655(98)00170-2, 1999.

Emery, C. M., Biancamaria, S., Boone, A., Garambois, P. A., Ricci, S., Rochoux, M. C., and Decharme, B.: Temporal Variance-Based Sensitivity Analysis of the River-Routing Component of the Large-Scale Hydrological Model ISBA-TRIP: Application on the Amazon Basin, J Hydrometeorol, 17, 3007-3027, 2016.

Espinoza, J. C., Ronchail, J., Guyot, J. L., Junquas, C., Vauchel, P., Lavado, W., Drapeau, G., and Pombosa, R.: Climate variability and extreme drought in the upper Solimões River (western Amazon Basin): Understanding the exceptional 2010 drought, Geophys Res Lett, 38, L13406, 2011.

Fearnside, P. M.: Deforestation in Brazilian Amazonia: History, rates, and consequences, Conserv Biol, 19, 680-688, 2005.

Gedeon, M., and Mallants, D.: Sensitivity Analysis of a Combined Groundwater Flow and Solute Transport Model Using Local-Grid Refinement: A Case Study, Mathematical Geosciences, 44, 881-899, 2012.

Hamby, D. M.: A review of techniques for parameter sensitivity analysis of environmental models, Environmental Monitoring and Assessment, 32, 135-154, 10.1007/bf00547132, 1994.

Helton, J. C., and Davis, F. J.: Latin hypercube sampling and the propagation of uncertainty in analyses of complex systems, Reliability Engineering & System Safety, 81, 23-69, 2003.

Hodnett, M. G., Vendrame, I., Marques, A. D., Oyama, M. D., and Tomasella, J.: Soil water storage and groundwater behaviour in a catenary sequence beneath forest in central Amazonia: I. Comparisons between plateau, slope and valley floor, Hydrol Earth Syst Sc, 1, 265-277, DOI 10.5194/hess-1-265-1997, 1997a.

https://doi.org/10.5194/hess-2020-87
Preprint. Discussion started: 10 March 2020


Hydrology and Earth System Sciences
Discussions

Hodnett, M. G., Vendrame, I., Marques, A. D., Oyama, M. D., and Tomasella, J.: Soil water storage and groundwater behaviour in a catenary sequence beneath forest in central Amazonia. II. Floodplain water table behaviour and implications for streamflow generation, Hydrol Earth Syst Sc, 1, 279-290, DOI 10.5194/hess-1-279-1997, 1997b.

Ji, X. Y., Shen, C. P., and Riley, W. J.: Temporal evolution of soil moisture statistical fractal and controls by soil texture and regional groundwater flow, Adv Water Resour, 86, 155-169, 10.1016/j.advwatres.2015.09.027, 2015.

Kanso, A., Chebbo, G., and Tassin, B.: Application of MCMC–GSA model calibration method to urban runoff quality modeling, Reliability Engineering & System Safety, 91, 1398-1405, 2006.

King, D. M., and Perera, B. J. C.: Morris method of sensitivity analysis applied to assess the importance of input variables on urban water supply yield – A case study, J Hydrol, 477, 17-32, 2013.

Leopoldo, P. R., Franken, W. K., and Villa Nova, N. A.: Real evapotranspiration and transpiration through a tropical rain forest in central Amazonia as estimated by the water balance method, Forest Ecology and Management, 73, 185-195, https://doi.org/10.1016/0378-1127(94)03487-H, 1995.

Lesack, L. F. W.: Water-Balance and Hydrologic Characteristics of a Rain-Forest Catchment in the Central Amazon Basin, Water Resour Res, 29, 759-773, Doi 10.1029/92wr02371, 1993.

Lesack, L. F. W., and Melack, J. M.: Mass balance of major solutes in a rainforest catchment in the Central Amazon: Implications for nutrient budgets in tropical rainforests, Biogeochemistry, 32, 115-142, 10.1007/bf00000355, 1996.

Lintner, B. R., Adams, D. K., Schiro, K. A., Stansfield, A. M., Rocha, A. A. A., and Neelin, J. D.: Relationships among climatological vertical moisture structure, column water vapor, and precipitation over the central Amazon in observations and CMIP5 models, Geophys Res Lett, 44, 2017.

Lu, D., Ye, M., and Hill, M. C.: Analysis of regression confidence intervals and Bayesian credible intervals for uncertainty quantification, Water Resour Res, 48, 10.1029/2011wr011289, 2012.

Makler-Pick, V., Gal, G., Gorfine, M., Hipsey, M. R., and Carmel, Y.: Sensitivity analysis for complex ecological models – A new approach, Environ Modell Softw, 26, 124-134, 2011.

Marengo, J. A., Liebmann, B., Kousky, V. E., Filizola, N. P., and Wainer, I. C.: Onset and end of the rainy season in the Brazilian Amazon Basin, J Climate, 14, 833-852, 2010.

Maxwell, R. M., Putti, M., Meyerhoff, S., Delfs, J. O., and Sulis, M.: Surface-subsurface model intercomparison: A first set of benchmark results to diagnose integrated hydrology and feedbacks, Water Resour Res, 50, 6641, 2014.

Mckay, M. D., Beckman, R. J., and Conover, W. J.: A Comparison of Three Methods for Selecting Values of Input Variables in the Analysis of Output from a Computer Code, Technometrics, 21, 239-245, 1979.

Meyer, P. D., Ye, M., Rockhold, M. L., Neuman, S. P., and Cantrell, K. J.: Combined Estimation of Hydrogeologic Conceptual Model, Parameter, and Scenario Uncertainty with Application to Uranium Transport at the Hanford Site 300 Area, Geosciences, 2007.

Miguez-Macho, G., and Fan, Y.: The role of groundwater in the Amazon water cycle: 1. Influence on seasonal streamflow, flooding and wetlands, Journal of Geophysical Research Atmospheres, 117, -, 2012a.

https://doi.org/10.5194/hess-2020-87
Preprint. Discussion started: 10 March 2020


Hydrology and Earth System Sciences
Discussions

555 Miguez-Macho, G., and Fan, Y.: The role of groundwater in the Amazon water cycle: 2. Influence on seasonal soil moisture and evapotranspiration, Journal of Geophysical Research Atmospheres, 117, -, 2012b.

Morley, R. J.: Origin and evolution of tropical rain forests, Origin & Evolution of Tropical Rain Forests, 15, 2000.

Mualem, Y.: A new model for predicting the hydraulic conductivity of unsaturated porous media, Water Resour Res, 12, 513-522, 10.1029/WR012i003p00513, 1976.

560 Neuman, S. P.: Maximum likelihood Bayesian averaging of uncertain model predictions, Stoch Env Res Risk A, 17, 291-305, 2003.

Neumann, M. B.: Comparison of sensitivity analysis methods for pollutant degradation modelling: a case study from drinking water treatment, Sci Total Environ, 433, 530-537, 2012.

Nijssen, B., O'Donnell, G. M., Hamlet, A. F., and Lettenmaier, D. P.: Hydrologic Sensitivity of Global Rivers to Climate
565 Change, Climatic Change, 50, 143-175, 2001.

Niu, J., and Phanikumar, M. S.: Modeling watershed-scale solute transport using an integrated, process-based hydrologic model with applications to bacterial fate and transport, J Hydrol, 529, 35-48, 10.1016/j.jhydrol.2015.07.013, 2015.

Niu, J., Shen, C. P., Li, S. G., and Phanikumar, M. S.: Quantifying storage changes in regional Great Lakes watersheds using a coupled subsurface-land surface process model and GRACE, MODIS products, Water Resour Res, 50, 7359-7377,
570 10.1002/2014wr015589, 2014.

Niu, J., Shen, C. P., Chambers, J. Q., Melack, J. M., and Riley, W. J.: Interannual Variation in Hydrologic Budgets in an Amazonian Watershed with a Coupled Subsurface-Land Surface Process Model, J Hydrometeorol, 18, 2597-2617, 10.1175/Jhm-D-17-0108.1, 2017.

Oliveira, R. S., Dawson, T. E., Burgess, S. S. O., and Nepstad, D. C.: Hydraulic redistribution in three Amazonian trees,
575 Oecologia, 145, 354-363, 10.1007/s00442-005-0108-2, 2005.

Owen, A. B.: Latin supercube sampling for very high-dimensional simulations, Acm Transactions on Modeling & Computer Simulation, 8, 71-102, 1998.

Pan, F., Zhu, J., Ye, M., Pachepsky, Y. A., and Wu, Y.-S.: Sensitivity analysis of unsaturated flow and contaminant transport with correlated parameters, J Hydrol, 397, 238-249, https://doi.org/10.1016/j.jhydrol.2010.11.045, 2011.

580 Pegoraro, E., Rey, A., Abrell, L., Vanharen, J., and Lin, G. H.: Drought effect on isoprene production and consumption in Biosphere 2 tropical rainforest, Global Change Biol, 12, 456-469, 2006.

Pelletier, J. D., Broxton, P. D., Hazenberg, P., Zeng, X., Troch, P. A., & Niu, G. Y., et al. (2016). A gridded global data set of soil, intact regolith, and sedimentary deposit thicknesses for regional and global land surface modeling. Journal of Advances in Modeling Earth Systems, 8(1), 41-65.

585 Phillips, O. L., Aragao, L. E., Lewis, S. L., Fisher, J. B., Lloyd, J., Lopez-Gonzalez, G., Malhi, Y., Monteagudo, A., Peacock, J., Quesada, C. A., van der Heijden, G., Almeida, S., Amaral, I., Arroyo, L., Aymard, G., Baker, T. R., Banki, O., Blanc, L., Bonal, D., Brando, P., Chave, J., de Oliveira, A. C., Cardozo, N. D., Czimczik, C. I., Feldpausch, T. R., Freitas, M. A., Gloor, E., Higuchi, N., Jimenez, E., Lloyd, G., Meir, P., Mendoza, C., Morel, A., Neill, D. A., Nepstad, D., Patino, S., Penuela, M.

C., Prieto, A., Ramirez, F., Schwarz, M., Silva, J., Silveira, M., Thomas, A. S., Steege, H. T., Stropp, J., Vasquez, R., Zelazowski, P., Alvarez Davila, E., Andelman, S., Andrade, A., Chao, K. J., Erwin, T., Di Fiore, A., Honorio, C. E., Keeling, H., Killeen, T. J., Laurance, W. F., Pena Cruz, A., Pitman, N. C., Nunez Vargas, P., Ramirez-Angulo, H., Rudas, A., Salamao, R., Silva, N., Terborgh, J., and Torres-Lezama, A.: Drought sensitivity of the Amazon rainforest, Science, 323, 1344-1347, 10.1126/science.1164033, 2009.

Piao, S. L., Ito, A., Li, S. G., Huang, Y., Ciais, P., Wang, X. H., Peng, S. S., Nan, H. J., Zhao, C., Ahlstrom, A., Andres, R. J., Chevallier, F., Fang, J. Y., Hartmann, J., Huntingford, C., Jeong, S., Levis, S., Levy, P. E., Li, J. S., Lomas, M. R., Mao, J. F., Mayorga, E., Mohammat, A., Muraoka, H., Peng, C. H., Peylin, P., Poulter, B., Shen, Z. H., Shi, X., Sitch, S., Tao, S., Tian, H. Q., Wu, X. P., Xu, M., Yu, G. R., Viovy, N., Zaehle, S., Zeng, N., and Zhu, B.: The carbon budget of terrestrial ecosystems in East Asia over the last two decades, Biogeosciences, 9, 3571-3586, 10.5194/bg-9-3571-2012, 2012.

Pokhrel, Y. N., Fan, Y., and Miguezmacho, G.: Potential Hydrologic Changes in the Amazon By the End of the 21st Century and the Groundwater Buffer, Environ Res Lett, 9, 084004, 2014.

Qiu H., Niu, J., and Phanikumar, M.S.: Quantifying the space – time variability of water balance components in an agricultural basin using a process-based hydrologic model and the Budyko framework, Science of The Total Environment, doi:10.1016/j.scitotenv.2019.04.147, 2019.

Razavi, S., and Gupta, H. V.: What do we mean by sensitivity analysis? The need for comprehensive characterization of "global" sensitivity in Earth and Environmental systems models, Water Resour Res, 51, 3070-3092, 2015.

Razavi, S., and Gupta, H. V.: A new framework for comprehensive, robust, and efficient global sensitivity analysis: 1. Theory, Water Resour Res, 52, 423-439, 2016.

Richey, J. E., Melack, J. M., Aufdenkampe, A. K., Ballester, V. M., and Hess, L. L.: Outgassing from Amazonian rivers and wetlands as a large tropical source of atmospheric CO2, Nature, 416, 617, 10.1038/416617a, 2002.

Riley, W. J., and Shen, C.: Characterizing coarse-resolution watershed soil moisture heterogeneity using fine-scale simulations, Hydrol. Earth Syst. Sci., 18, 2463-2483, 10.5194/hess-18-2463-2014, 2014.

Rojas, R., Kahunde, S., Peeters, L., Batelaan, O., Feyen, L., and Dassargues, A.: Application of a multimodel approach to account for conceptual model and scenario uncertainties in groundwater modelling, J Hydrol, 394, 416-435, https://doi.org/10.1016/j.jhydrol.2010.09.016, 2010.

Saltelli, A., and Sobol, I. M.: About the use of rank transformation in sensitivity analysis of model output, Reliability Engineering & System Safety, 50, 225-239, 1995.

Saltelli, A., Chan, K., and Scott, E. M.: Sensitivity Analysis, 2000.

Saltelli, A., Annoni, P., Azzini, I., Campolongo, F., Ratto, M., and Tarantola, S.: Variance based sensitivity analysis of model output. Design and estimator for the total sensitivity index, Comput Phys Commun, 181, 259-270, 2010.

Schoniger, A., Wohling, T., Samaniego, L., and Nowak, W.: Model selection on solid ground: Rigorous comparison of nine ways to evaluate Bayesian model evidence, Water Resour Res, 50, 9484-9513, 2014.

https://doi.org/10.5194/hess-2020-87
Preprint. Discussion started: 10 March 2020

Shen, C. P., and Phanikumar, M. S.: A process-based, distributed hydrologic model based on a large-scale method for surface-subsurface coupling, Adv Water Resour, 33, 1524-1541, 10.1016/j.advwatres.2010.09.002, 2010.

Shen, C., Jie, N., and Phanikumar, M. S.: Evaluating controls on coupled hydrologic and vegetation dynamics in a humid continental climate watershed using a subsurface-land surface processes model, Water Resour Res, 49, 2552–2572, 2013.

Shen, C., Jie, N., and Fang, K.: Quantifying the effects of data integration algorithms on the outcomes of a subsurface-land surface processes model, Environ Modell Softw, 59, 146-161, 2014.

Shen, C. P., Riley, W. J., Smithgall, K. R., Melack, J. M., and Fang, K.: The fan of influence of streams and channel feedbacks to simulated land surface water and carbon dynamics, Water Resour Res, 52, 880-902, 10.1002/2015wr018086, 2016.

Song, X., Zhang, J., Zhan, C., Xuan, Y., Ye, M., and Xu, C.: Global sensitivity analysis in hydrological modeling: Review of concepts, methods, theoretical framework, and applications, J Hydrol, 523, 739-757, 2015.

Sorribas, M. V., Paiva, R. C. D., Melack, J. M., Bravo, J. M., Jones, C., Carvalho, L., Beighley, E., Forsberg, B., and Costa, M. H.: Projections of climate change effects on discharge and inundation in the Amazon basin, Climatic Change, 136, 555-570, 10.1007/s10584-016-1640-2, 2016.

Sulis, M., Paniconi, C., Rivard, C., Harvey, R., and Chaumont, D.: Assessment of climate change impacts at the catchment scale with a detailed hydrological model of surface-subsurface interactions and comparison with a land surface model, Water Resour Res, 47, doi:10.1029/2010WR009167, 2011.

Tang, J., Riley, W. J., and Niu, J.: Incorporating root hydraulic redistribution in CLM4.5: Effects on predicted site and global evapotranspiration, soil moisture, and water storage, Journal of Advances in Modeling Earth Systems, 7, 1828-1848, 2015.

Tomasella, J., Hodnett, M. G., Cuartas, L. A., Nobre, A. D., Waterloo, M. J., and Oliveira, S. M.: The water balance of an Amazonian micro-catchment: the effect of interannual variability of rainfall on hydrological behaviour, Hydrol Process, 22, 2133-2147, doi:10.1002/hyp.6813, 2008.

van Dam, J. C., and Feddes, R. A.: Numerical simulation of infiltration, evaporation and shallow groundwater levels with the Richards equation, J Hydrol, 233, 72-85, Doi 10.1016/S0022-1694(00)00227-4, 2000.

van Genuchten, M. T.: A Closed-form Equation for Predicting the Hydraulic Conductivity of Unsaturated Soils1, Soil Sci Soc Am J, 44, 892-898, 10.2136/sssaj1980.03615995004400050002x, 1980.

van Griensven, A., Meixner, T., Grunwald, S., Bishop, T., Diluzio, M., and Srinivasan, R.: A global sensitivity analysis tool for the parameters of multi-variable catchment models, J Hydrol, 324, 10-23, https://doi.org/10.1016/j.jhydrol.2005.09.008, 2006.

Wainwright, H. M., Finsterle, S., Jung, Y., Zhou, Q., and Birkholzer, J. T.: Making sense of global sensitivity analyses, Computers & Geosciences, 65, 84-94, 2014.

Yamazaki, D., Lee, H., Alsdorf, D. E., Dutra, E., Kim, H., Kanae, S., and Oki, T.: Analysis of the water level dynamics simulated by a global river model: A case study in the Amazon River, Water Resour Res, 48, 2012.

https://doi.org/10.5194/hess-2020-87
Preprint. Discussion started: 10 March 2020


Hydrology and Earth System Sciences
Discussions

655 Ye, M., S. P. Neuman, P. D. Meyer, and Pohlmann. K. F.: Sensitivity analysis and assessment of prior model probabilities in MLBMA with application to unsaturated fractured tuff, Water Resour. Res., 41, W12429, 2005.

Ye, M., K. F. Pohlmann, and Chapman J. B.: Expert elicitation of recharge model probabilities for the Death Valley regional flow system, J. Hydrol, 354, 102-115, 2008.

Zhang, Y. Q., and Pinder, G.: Latin hypercube lattice sample selection strategy for correlated random hydraulic conductivity
660 fields, Water Resour Res, 39, 2003.

Zhang, C., Chu, J., and Fu, G.: Sobol''s sensitivity analysis for a distributed hydrological model of Yichun River Basin, China, J Hydrol, 480, 58-68, https://doi.org/10.1016/j.jhydrol.2012.12.005, 2013.

https://doi.org/10.5194/hess-2020-87
Preprint. Discussion started: 10 March 2020

Hydrology and Earth System Sciences
Discussions

665

Table 1. Statistical information for the daily data for the six climate scenarios. Here, μ represents the mean value and σ represents the standard deviation.

	Wet season			**Dry season**		
climate scenarios	CS_1	CS_2	CS_3	CS_4	CS_5	CS_6
precipitation (μ [mm], σ)	(10.96, 2.78)	(9.49, 2.8)	(7.87, 2.91)	(4.84, 1.81)	(3.99, 1.62)	(3.38, 1.35)
maximum temperature (μ [°C], σ)	(29.33, 0.66)	(29.94, 0.60)	(30.03, 0.62)	(30.80, 0.65)	(30.80,1.03)	(31.50, 1.04)
minimum temperature (μ [°C], σ)	(25.13, 0.54)	(25.63, 0.55)	(25.74, 0.48)	(25,59, 0.77)	(25.47, 0.81)	(26.02, 0.82)
radiation intensity (μ [MJ m^{-2}], σ)	(3973.5, 129.6)	(3975.1, 122.9)	(3982.4, 113.6)	(4285.5, 199.1)	(4299.5, 195.6)	(4312.1, 215.8)
relative humidity (μ [unitless], σ)	(0.0188, 4.65e-4)	(0.0191, 3.54e-4)	(0.0192, 4.72e-4)	(0.0186, 5.44e-4)	(0.0185, 5.76e-4)	(0.0188, 5.75e-4)
average wind speed (μ [m s^{-1}], σ)	(0.595, 0.122)	(0.648, 0.141)	(0.642, 0.148)	(0.549, 0.073)	(0.518, 0.061)	(0.552, 0.081)

https://doi.org/10.5194/hess-2020-87
Preprint. Discussion started: 10 March 2020

Hydrology and Earth System Sciences
Discussions

Table 2. Six chosen parameters to be included in parameter uncertainty

Group	Parameter	Unit	Description	Allowable Range
vadose zone (**PR**$_{VDZ}$)	K_s	m day^{-1}	soil saturated hydraulic conductivity	0.0-10.0
	α	m^{-1}	Van Genuchten parameter	0.1-4.0
	N		Van Genuchten parameter	1.03-5.0
groundwater (**PR**$_{GW}$)	K_1	m day^{-1}	unconfined aquifer hydraulic conductivity	0.0-60.0
	K_2	m day^{-1}	confined aquifer hydraulic conductivity	0.0-10.0
overland flow (**PR**$_{OVN}$)	L	m	length of flow path for runoff contribution to the overland flow domain	20.0-700.0

https://doi.org/10.5194/hess-2020-87
Preprint. Discussion started: 10 March 2020

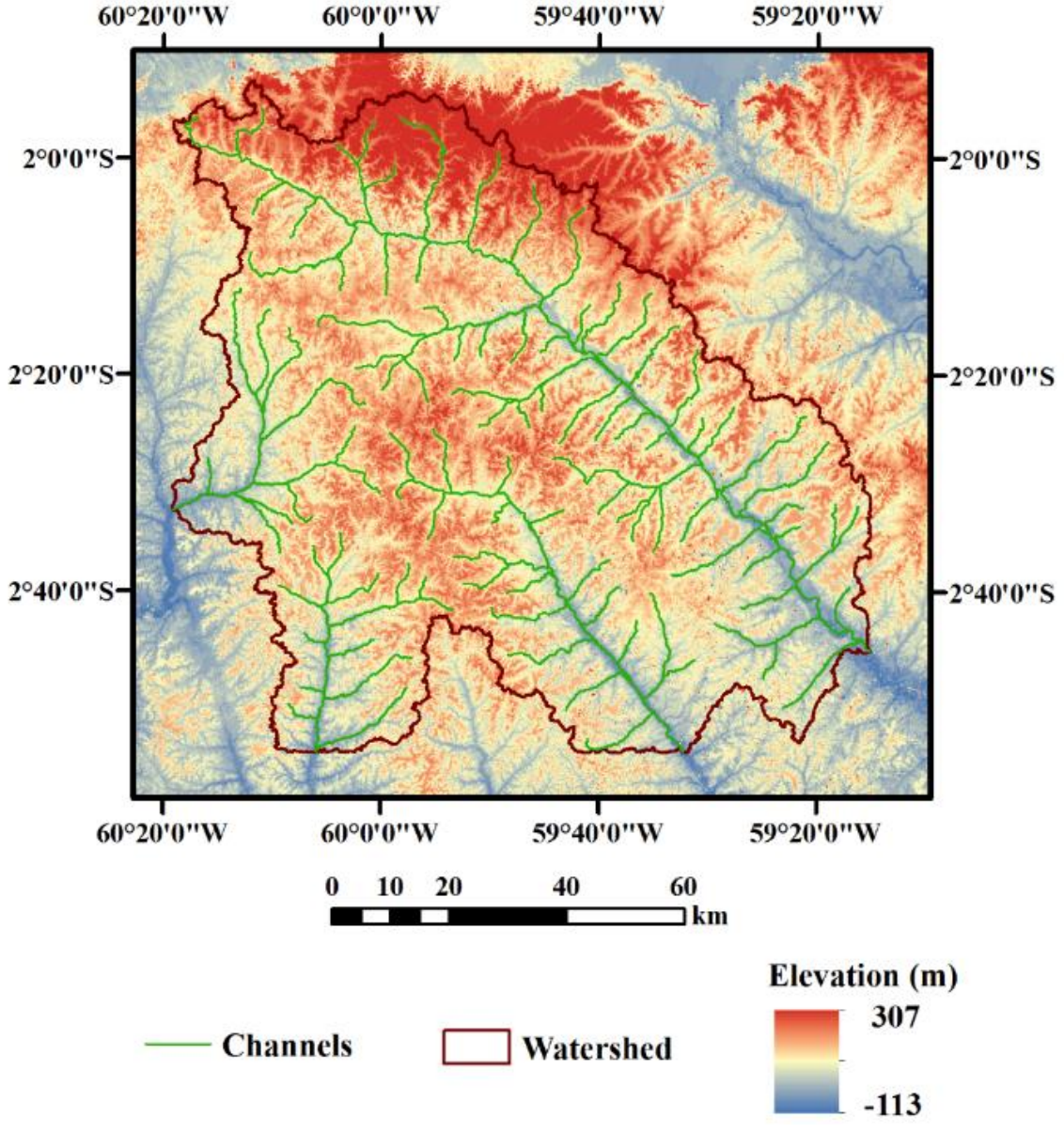

Figure 1. 2-D map of the watershed used in this study, showing the elevation, channels and watershed boundary. The study area extends from 1°57′36″S to 2°56′0″W and 59°14′48″W to 60°20′0″W.

675

https://doi.org/10.5194/hess-2020-87
Preprint. Discussion started: 10 March 2020

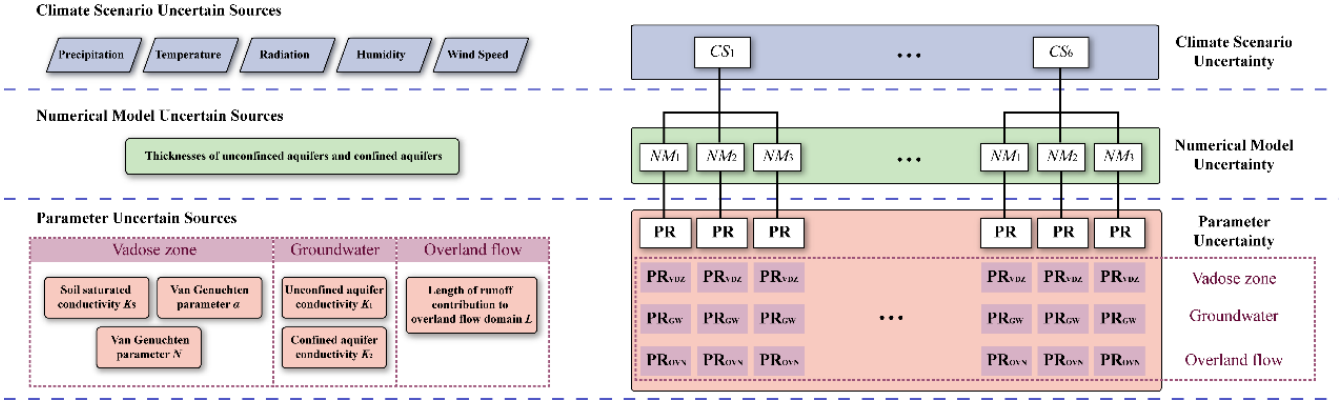

Figure 2. The framework of the hierarchical sensitivity analysis developed for PAWS applied to the central Amazon basins. The three uncertainty source types are placed into the appropriate hierarchical level according to their dependence relationships. The left part of this figure shows the sources of these uncertainties, and the right side shows the abbreviations and the structural relationships among the various uncertainties. The number of climate scenarios in this study is six; the number of plausible numerical models under each climate scenario is three; and the number of parameter sets under each numerical model is 600. It should be noted that the parameter uncertainty sources are further divided into three parts: vadose zone parameters, groundwater parameters and the overland flow parameter.

https://doi.org/10.5194/hess-2020-87
Preprint. Discussion started: 10 March 2020

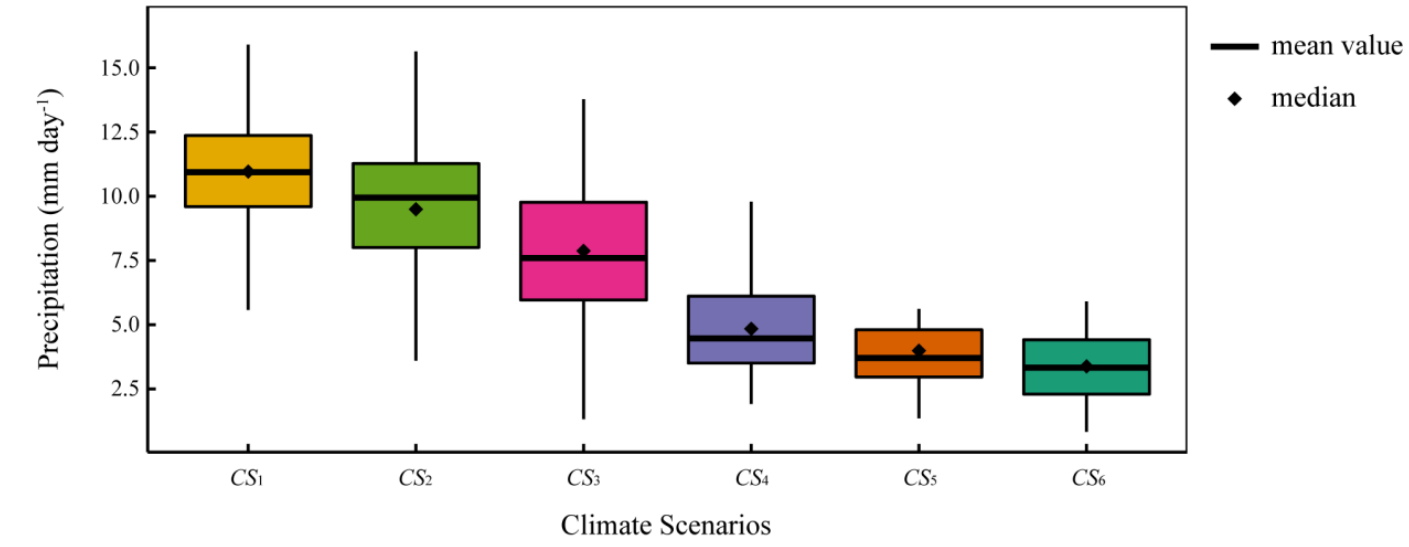

Figure 3. We identified six climate scenarios based on precipitation data for 1998-2013 from NASA's Tropical Measuring Mission (TRMM) data (http://trmm.gsfc.nasa.gov/). The first climate scenario (CS_1) is the wettest one, and the sixth climate scenario (CS_6) is the driest one.

https://doi.org/10.5194/hess-2020-87
Preprint. Discussion started: 10 March 2020

Hydrology and Earth System Sciences
Discussions

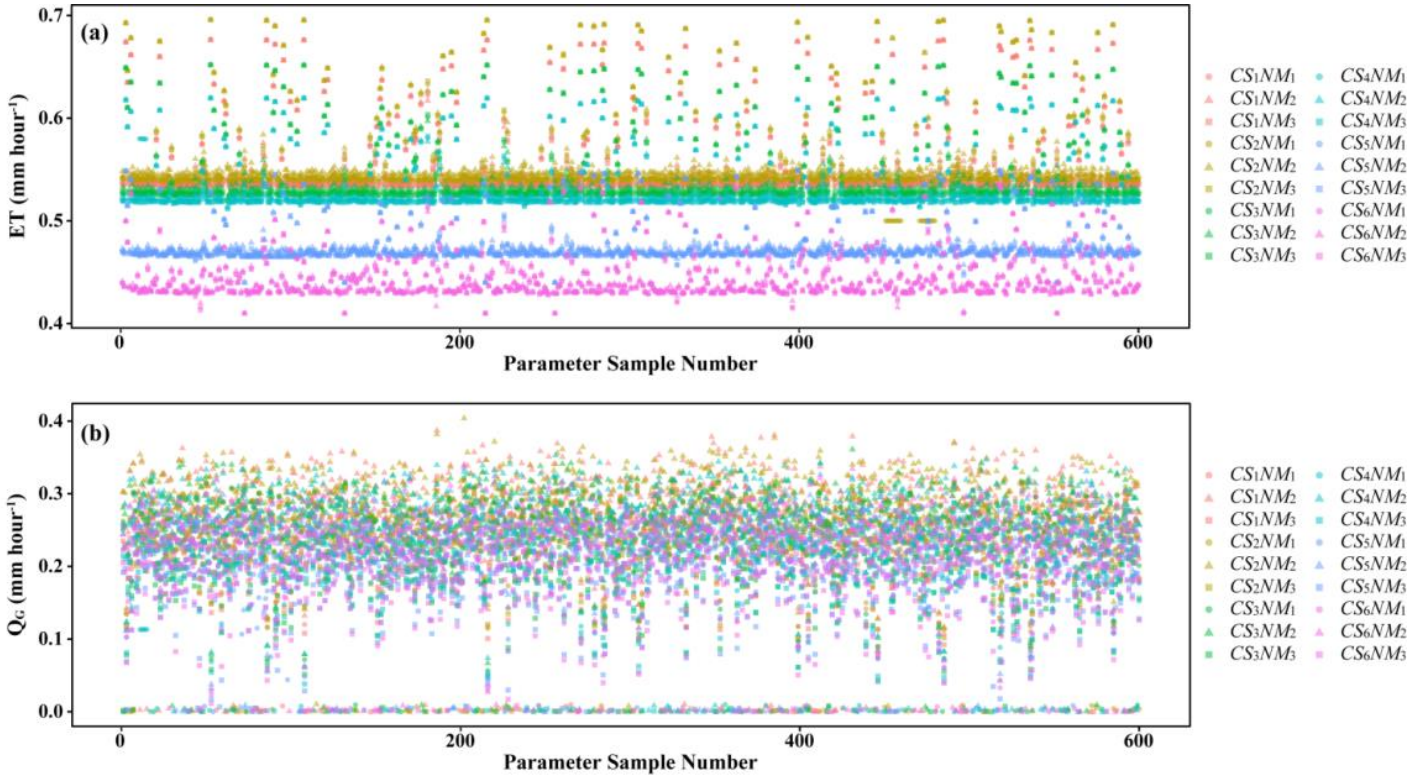

Figure 4. The spatially averaged outputs for evapotranspiration (*ET*) (a) and groundwater contribution to stream flow (Q_G) (b) at 2868 hours (at 12:00 wall-clock time). The x-axis represents the 600 parameter samples. The different climate scenarios are represented with different colours, and the different numerical models are represented with different shapes.

https://doi.org/10.5194/hess-2020-87
Preprint. Discussion started: 10 March 2020

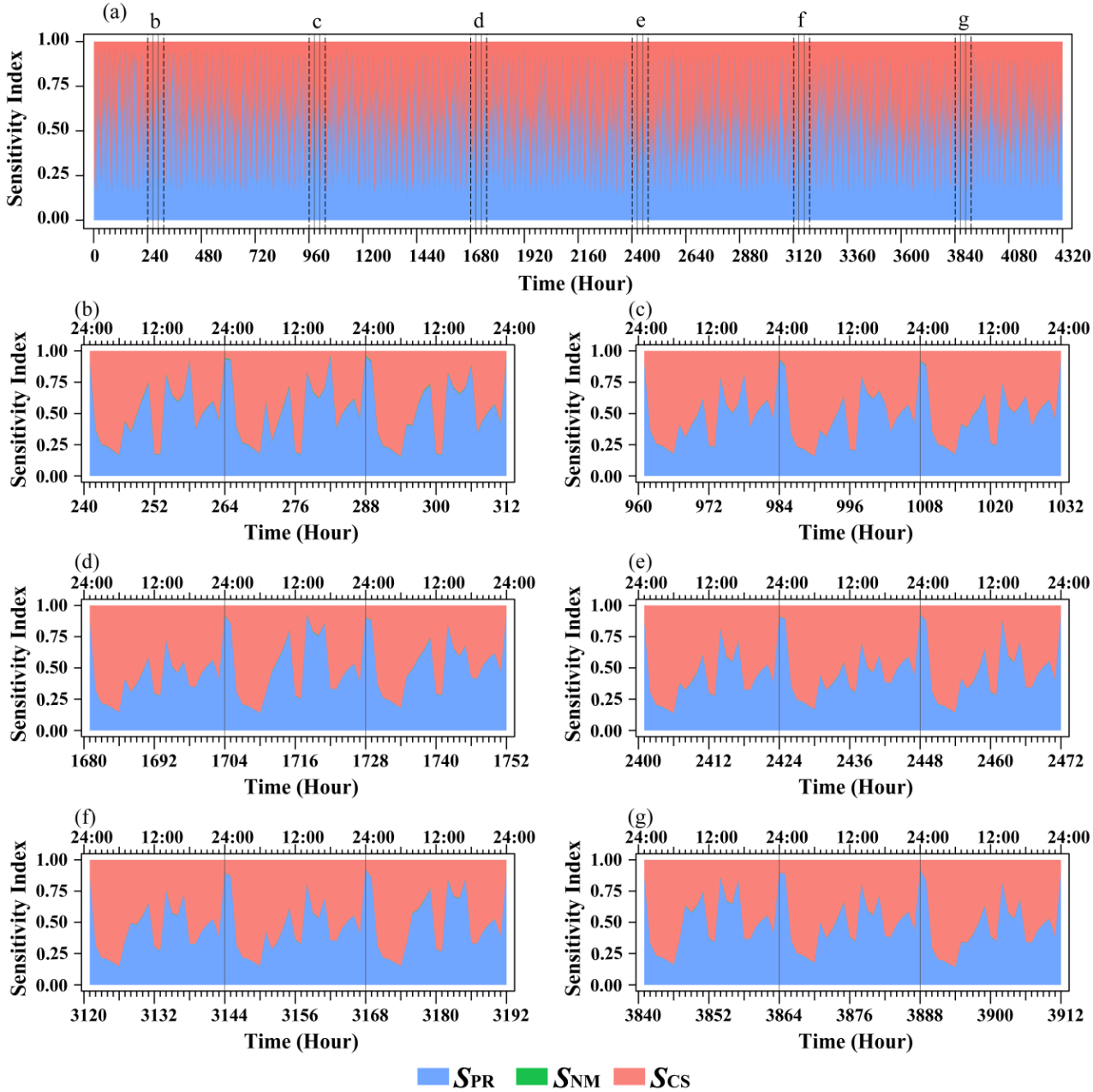

Figure 5. Estimated sensitivities for the spatially averaged evapotranspiration (*ET*) at whole time steps (a). We chose six periods at three-day intervals to display the sensitivity index values in detail. The bottom six figures exhibit the sensitivity index results for 241-312 hours (b), 961-1032 hours (c), 1681-1752 hours (d), 2401-2472 hours (e), 3121-3192 hours (f), and 3841-3912 hours (g). S_{PR} is the sensitivity index for parameters. S_{NM} is the sensitivity index for models and represents the influence of aquifer thickness. S_{CS} is the sensitivity index for climate scenarios. The bottom x-axis of (b)-(g) represents the simulated time steps, and the upper x-axis of (b)-(g) represents the local time.

https://doi.org/10.5194/hess-2020-87
Preprint. Discussion started: 10 March 2020

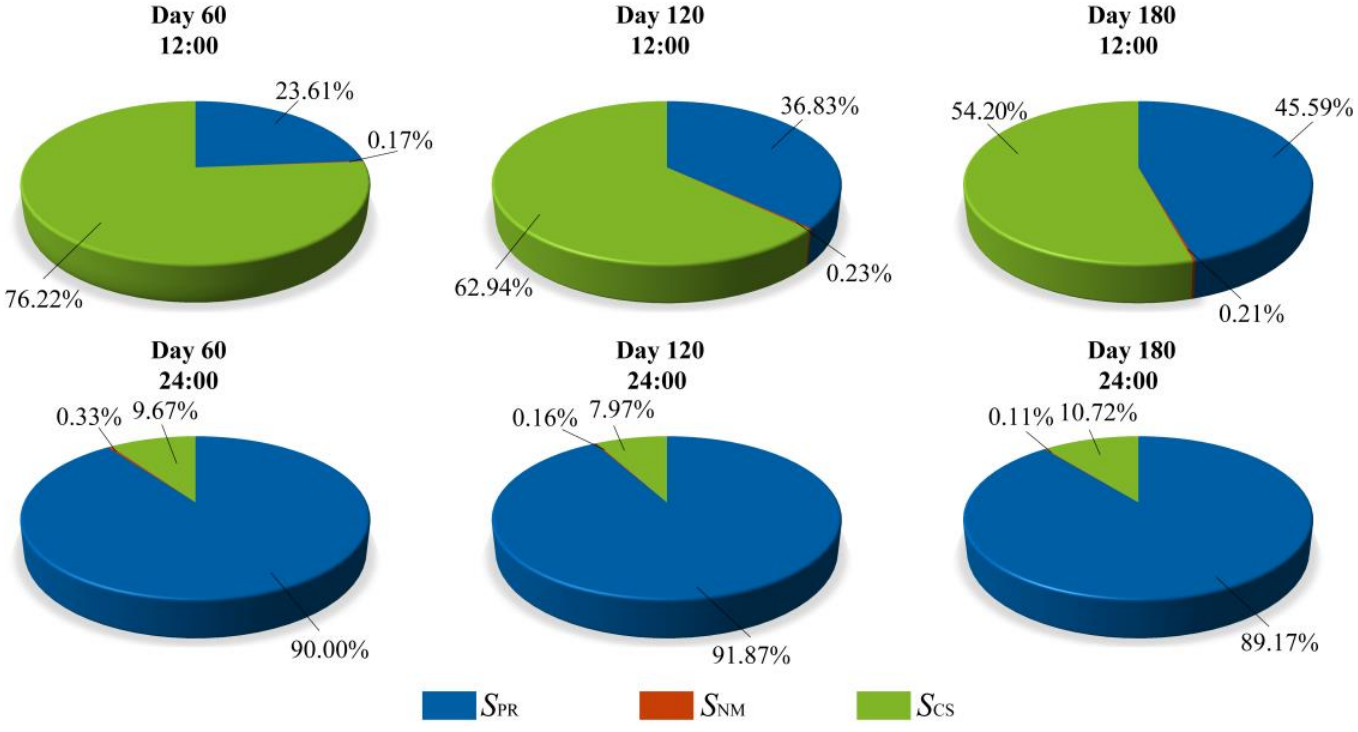

Figure 6. Estimated sensitivities for the spatially averaged evapotranspiration (*ET*) at 6 time points (simulation times = 1428 hour (Day 60, 12:00), 1440 hour (Day 60, 24:00), 2868 hour (Day 120, 12:00), 2880 hour (Day 120, 24:00), 4308 hour (Day 180, 12:00), and 4320 hour (Day 180, 24:00)). S_{PR} is the sensitivity index for the parameters. S_{NM} is the sensitivity index for the numerical models, and S_{CS} is the sensitivity index for the climate scenarios.

https://doi.org/10.5194/hess-2020-87
Preprint. Discussion started: 10 March 2020

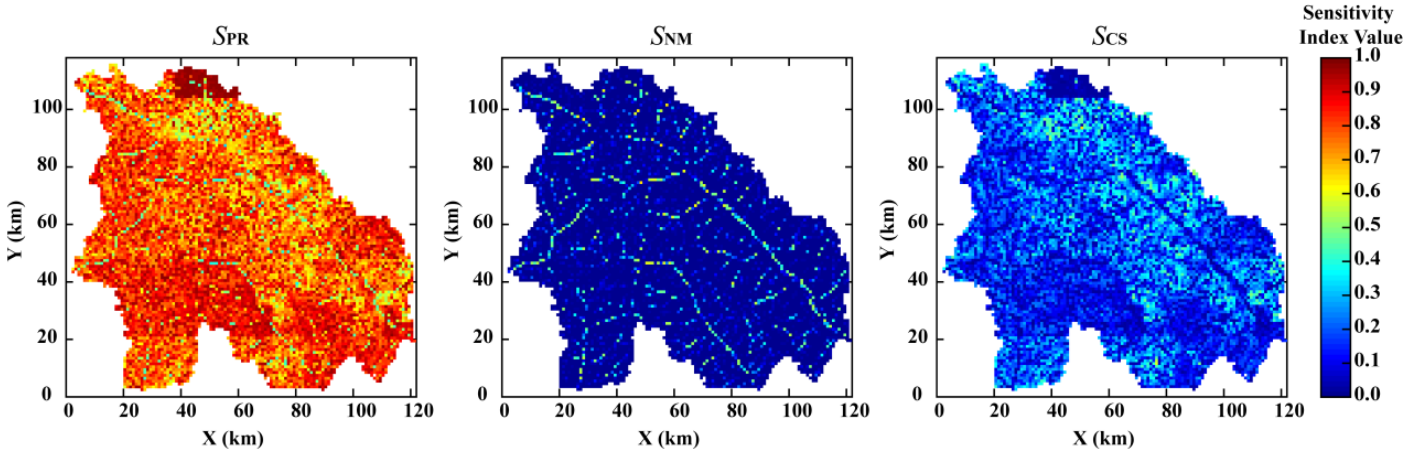

Figure 7. Maps of parametric (S_{PR}), numerical model (S_{NM}), and climate scenario (S_{CS}) sensitivity index values for time-averaged evapotranspiration (ET) predictions.

https://doi.org/10.5194/hess-2020-87
Preprint. Discussion started: 10 March 2020

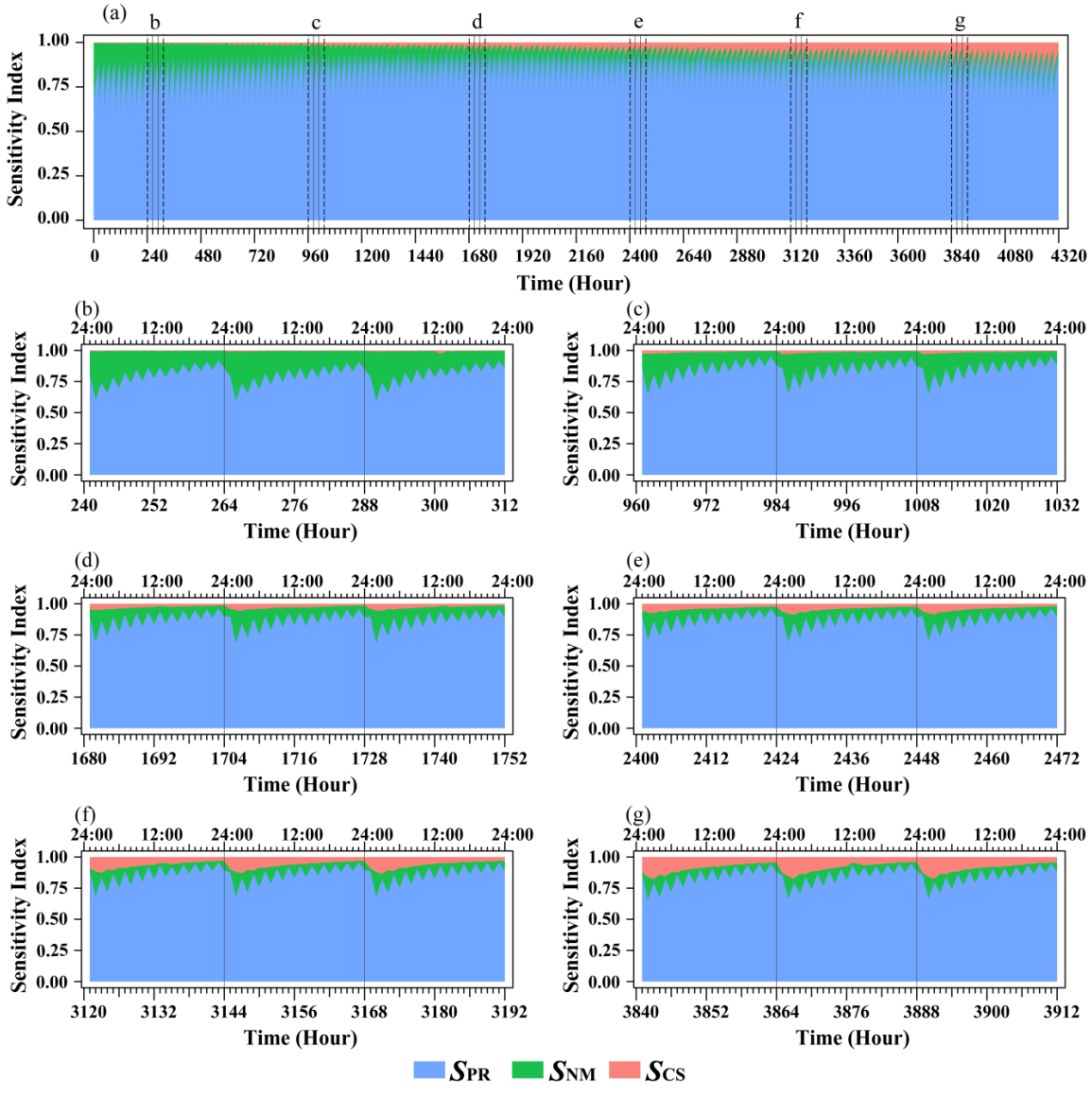

Figure 8. Estimated sensitivities for the spatially averaged groundwater contribution to stream flow (Q_G) at whole time steps (a). We chose six periods at three-day intervals to display the sensitivity index values in detail. The bottom six figures exhibit the sensitivity index results for 241-312 hours (b), 961-1032 hours (c), 1681-1752 hours (d), 2401-2472 hours (e), 3121-3192 hours (f), and 3841-3912 hours (g). S_{PR} is the sensitivity index for parameters. S_{NM} is the sensitivity index for models and represents the influence of aquifer thickness. S_{CS} is the sensitivity index for climate scenarios. The bottom x-axis of (b)-(g) represents the simulated time steps, and the upper x-axis of (b)-(g) represents the local time.

https://doi.org/10.5194/hess-2020-87
Preprint. Discussion started: 10 March 2020

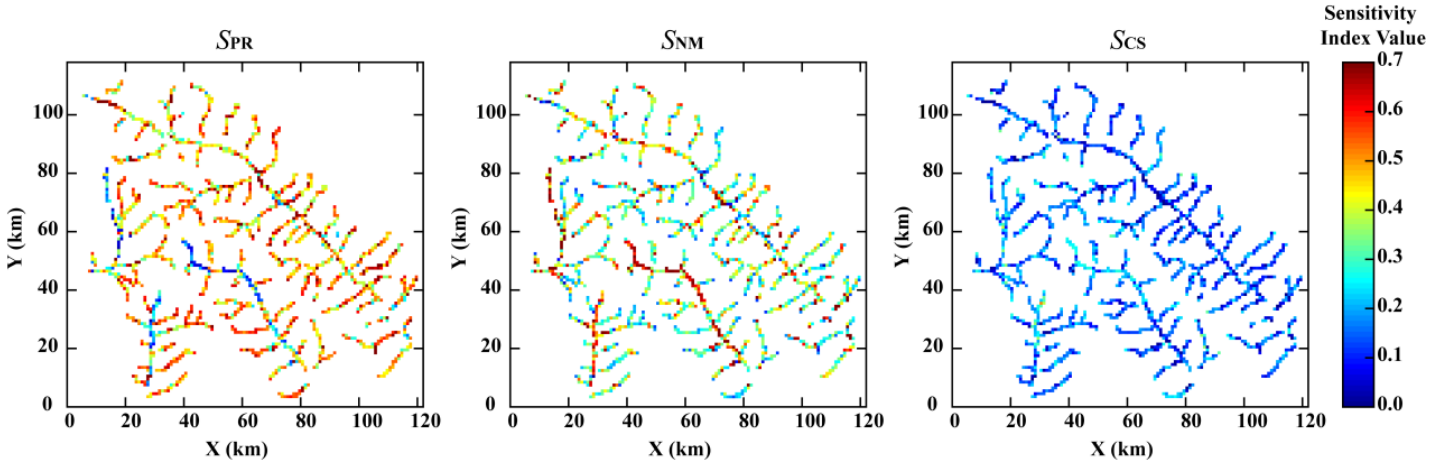

Figure 9. Maps of parametric sensitivity indices (S_{PR}), numerical model sensitivity indices (S_{NM}), and climate scenario sensitivity indices (S_{CS}) for the time-averaged groundwater contribution to stream flow (Q_G) predictions.

https://doi.org/10.5194/hess-2020-87
Preprint. Discussion started: 10 March 2020

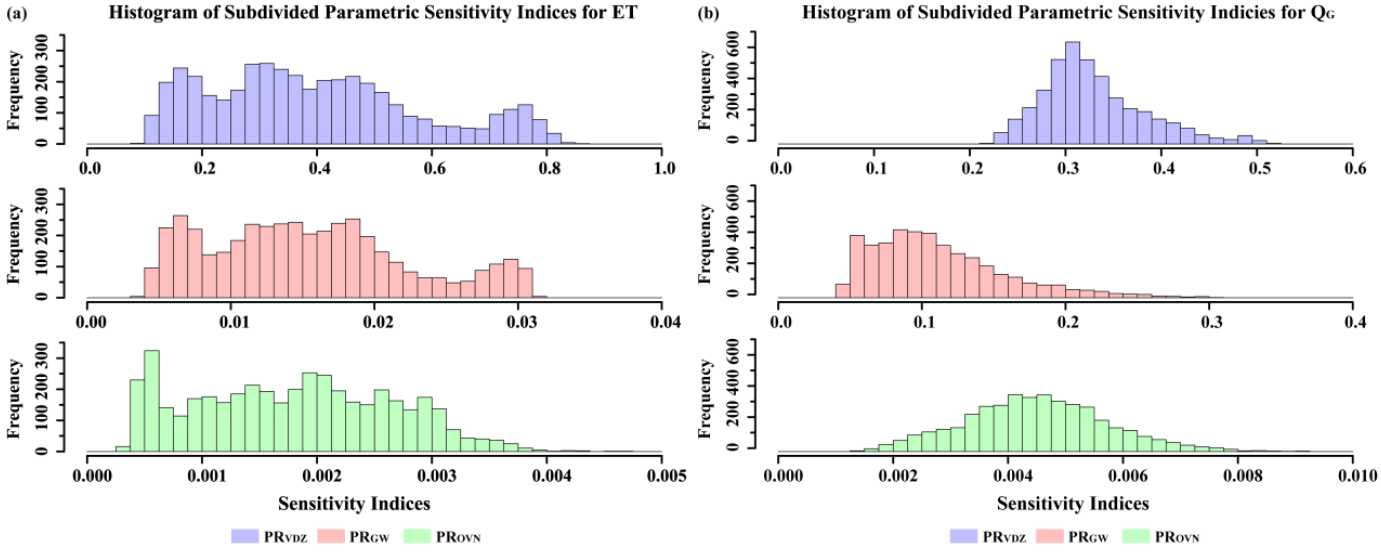

Figure 10. Frequency histograms of subdivided parametric sensitivity indices for spatially averaged results over all 4320 time steps. The results for evapotranspiration (*ET*) as our output are depicted in (a), and the results for groundwater contribution to stream flow (Q_G) as our output are depicted in (b). PR_{VDZ} represents the vadose zone parameters. PR_{GW} represents the groundwater parameters. PR_{OVN} represents the overland flow parameter.

https://doi.org/10.5194/hess-2020-87
Preprint. Discussion started: 10 March 2020

Hydrology and Earth System Sciences
Discussions
Open Access
EGU

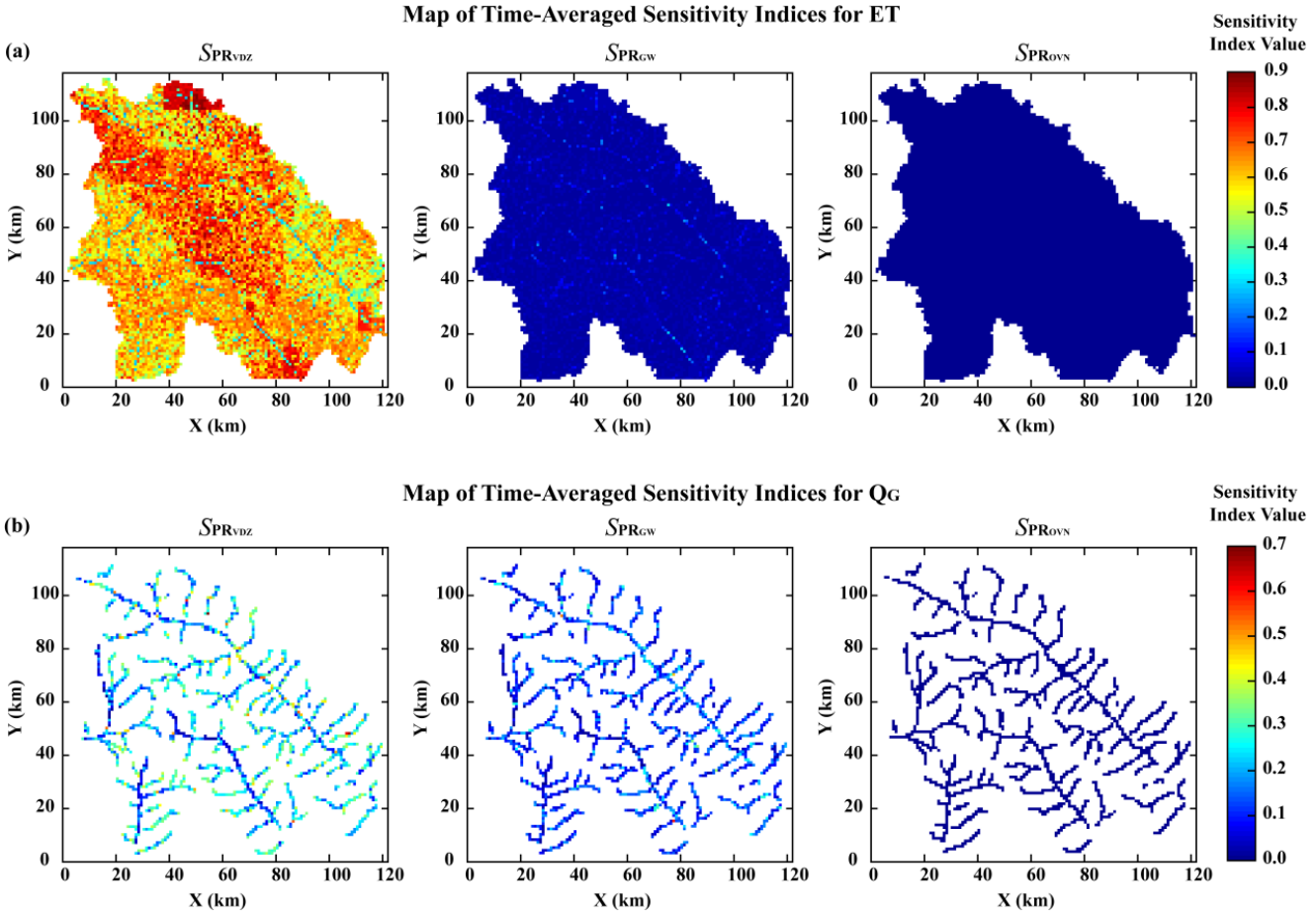

Figure 11. Maps of vadose zone parameter sensitivity indices ($S_{PR_{VDZ}}$), groundwater parameter sensitivity indices ($S_{PR_{GW}}$) and overland flow parameter sensitivity indices ($S_{PR_{OVN}}$) for time-averaged evapotranspiration (*ET*) (a) and groundwater contribution to stream flow (Q_G) (b) predictions.

https://doi.org/10.5194/hess-2020-87
Preprint. Discussion started: 10 March 2020

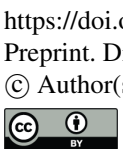

Hydrology and Earth System Sciences
Discussions

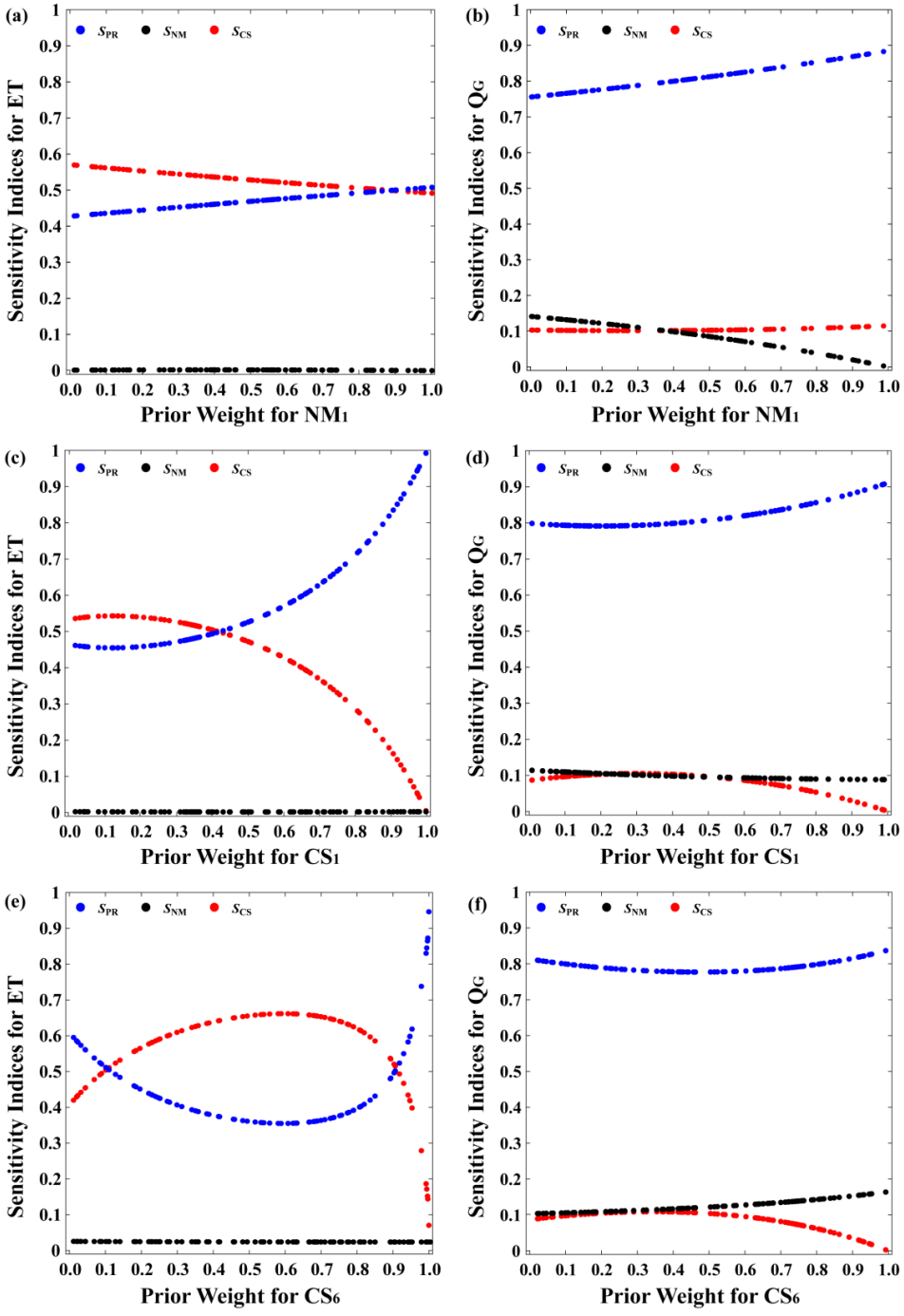

735

Figure 12. Patterns of S_{PR}, S_{NM}, and S_{CS} for space-averaged evapotranspiration (*ET*) and space-averaged groundwater contribution to stream flow (Q_G) with changes in the prior weights of numerical model NM_1, climate scenario CS_1 and climate scenario CS_6 at the time step of 4308 hours (at 12:00 wall-clock time).